

K55 10

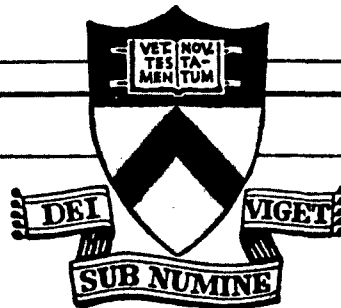
N 7 2 2 9 2 0 5

HOLLOW CATHODE, QUASI-STEADY

MPD ARC

N. Parmentier and R. G. Jahn

Report 1023



CASE FILE
COPY

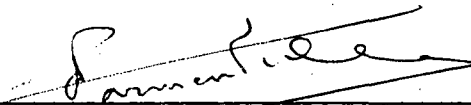
PRINCETON UNIVERSITY
DEPARTMENT OF
AEROSPACE AND MECHANICAL SCIENCES

Prepared for
National Aeronautics
and Space Administration
NASA Research Grant NGL 31-001-005

HOLLOW CATHODE, QUASI-STEADY
MPD ARC

N. Parmentier and R. G. Jahn

Report 1023

Prepared by 
Noel Parmentier

Approved by 
R. G. Jahn
Dean, School of Engineering

*This report is a reproduction in entirety of the M.S.E. dissertation of Mr. Noel Parmentier. It is submitted to the sponsor and to the distribution list in this form both as a presentation of the technical material, and as an indication of the academic program supported by this Grant.

Reproduction, translation, publication, use and disposal in whole, or in part, by or for the United States Government is permitted.

December 1971

Department of Aerospace and Mechanical Sciences
PRINCETON UNIVERSITY
Princeton, New Jersey

Abstract

A quasi-steady MPD accelerator has been operated with four different hollow cathodes over a power range from 5 kilowatts to 5 megawatts. The absolute level of the argon mass flow, as well as the fractional division of the flow between the cathode and the six standard chamber injectors, is varied over a range of 1 to 12 grams per second. For a fixed total current, it is observed that the voltage increases monotonically with mass flow rate, compared to the usual experience with solid cathodes where the voltage decreases with mass flow rate. For a fixed percentage of flow through the cathode, each hollow cathode configuration displays a minimum impedance at a particular value of the total mass flow. It is asserted that in order to keep the discharge inside the hollow cathode the magnetic pressure and gasdynamic pressure have to match inside the cavity.

ACKNOWLEDGEMENTS

The author gratefully acknowledges the support of NASA Research Grant NGL 31-001-005 in making this research possible. The advice and encouragement given by Professor Robert G. Jahn, Senior Research Engineer Woldemar F. von Jaskowsky, and Research Staff Member Kenn E. Clark, are deeply appreciated. Thanks are also given to all the other members of the Electric Propulsion Laboratory, especially Mr. A. J. Saber, for their help in this work.

Thanks are given to the National Academy of Sciences, NASA, and European Space Research Organization for awarding the author a Graduate Fellowship; without this aid, graduate studies would not have been possible.

TABLE OF CONTENTS

	<u>Page</u>
TITLE PAGE.	i
ABSTRACT.	ii
ACKNOWLEDGEMENTS.	iii
TABLE OF CONTENTS	iv
LIST OF ILLUSTRATIONS	v
TABLES.	v
NOMENCLATURE.	vi
CHAPTER	
I. INTRODUCTION	1
II. BACKGROUND AND LITERATURE SURVEY OF PREVIOUS WORK.	3
A. Physical Processes in Hollow Cathodes and Design Criteria	3
B. Hollow Cathode Performance Parameters	5
C. Criteria for Hollow Cathode Operation	8
III. STUDY OF HOLLOW CATHODE MPD DISCHARGE. . . .	10
A. Apparatus and Hollow Cathode Design	10
B. Discharge Characteristics	21
C. Dynamic Behavior of Discharge Voltage and Current	41
IV. DISCUSSION	46
A. Magnetic Pressure	46
B. Gasdynamic Pressure	49
V. SUMMARY.	54
APPENDIX: Calculation of the Mean Free-Path	55
REFERENCES: Hollow Cathode	58
REFERENCES: General	63

LIST OF ILLUSTRATIONS

	<u>Page</u>
1. Hollow cathode experimental configuration	11
2. Arrangement for Kerr-cell photography	13
3. Typical current and voltage record, electrolytic bank	14
4. Cathode configurations	16
5. Hollow cathode current pattern	17
6. Tungsten hollow cathode (HC-W) and discharge chamber geometry	22
7. Discharge characteristics of solid conical and cylindrical hollow cathode (HC-SS)	23
8. HC-SS discharge characteristics	25
9. HC-W characteristics	26
10. Tungsten solid conical cathode characteristics	27
11. HC-W characteristics	28
12. Influence of % mass flow inside on the discharge voltage	30
13. HC-SS discharge	31
14. Summary of discharge characteristics of insulated hollow cathode	34
15. Discharge current - mass flow characteristic of cylindrical hollow cathode	35
16. Discharge mass flow characteristics of insulated hollow cathode	36
17. HC-W mass flow characteristics	39
18. Discharge current - mass flow characteristics of the conical hollow cathode	40
19. Characteristics for optimum mass flows	42
20. Voltage and current profiles, electrolytic capacitor bank	43
21. HC-W current and voltage profiles, high-voltage capacitor bank	45
22. Discharge with conical hollow cathode	47
23. Kerr-cell photographs of HC-INS discharge	50
24. Starting sequence with tungsten hollow cathode	52

TABLE

I. Comparison of Hollow Cathode Parameters	7
--	---

NOMENCLATURE (Cont'd)

Subscripts (Cont'd)

e electron
i inside
o total
r radial
s surface
t threshold
+ anode

Superscripts

i ionization

rate at the cathode surface and therefore the erosion will be lower for a hollow cathode at comparable other operating conditions. Thus the magnitude and the location of the cathode fall will have a major influence on cathode lifetime.

The ultimate goal of this work was a further understanding of the proper working mechanism and scaling parameters correlating the total current and mass flow with the dimensions for the hollow cathode.

In an exploratory series of experiments, the standard solid conical cathode was replaced by one of four different hollow cathodes of different dimensions and materials over a power range from 5 kW to 5 MW. The absolute level of the mass flow, as well as the fractional division of the flow through the cathode and the six standard chamber injectors, was varied. Determination of cathode operating characteristics of terminal arc voltage as a function of arc current and mass flow were thought to be important for two reasons. First, the characteristics would bring into evidence any major differences between the discharge mechanism of conventional and hollow cathode MPD arcs. Second, they would indicate whether the efficient hollow cathode mechanism could be used advantageously in high power MPD arcs.

In an investigation of the current attachment at the cathode, Kerr-cell photographs of the discharge were taken both during the starting transient and steady regions.

CHAPTER II

BACKGROUND AND LITERATURE SURVEY OF PREVIOUS WORK

A. Physical Processes in Hollow Cathodes and Design Criteria

For a low current discharge the plasma inside a hollow cathode represents a positive column modified by injection of electrons from the cathode fall region. The Faraday dark space may be absent, and in this case the discharge in the cathode consists of two regions only; a dark cathode space and a luminous positive column. This column may be either uniform or striated. It has been shown^{11,12} that in a hollow cathode discharge most of the excitation and the ionization processes occur in the negative glow. This region is characterized by an equipotential plasma through which travel the relatively few, but energetic, electrons originating in cathodic processes. Randomly moving secondary electrons generated in the plasma are responsible for most of the excitation processes in the glow. The dark space plays only the role of a primary electron gun conferring to the electrons the energy required for maintaining the discharge.^{A-1}

The discharge of a hollow cathode of the type used in ion thrusters can be distinguished by two different modes of operation, the plume mode and the spot mode.^{18,19,23,24,27} The plume mode has a low electron number density and a high discharge resistance. In this mode a sheath is formed in front of the hollow cathode, and only a few of the electrons are accelerated through it to collide with neutrals and ionize them near the cathode. Fast electrons may then leave the neighborhood of the cathode and cause some ionization and excitation in the region between cathode and anode. This mechanism is thought to be the cause of the luminous plume in

the discharge. The spot mode, however, has a lower discharge resistance, and it is necessary to assume that the sheath edge forms deep enough in the cathode to trap most electrons leaving the sheath in the cavity. This allows electrons accelerated through the sheath to ionize before they leave the high neutral density region. This region of potential gradient, or "sheath" has a thickness approximately equal to the Debye length,

$$\ell_D = 69 \left(\frac{T_e}{n_e} \right)^{1/2} \quad [mks] \quad (II-1)$$

where T_e is the electron temperature, and n_e is the electron number density.^{2,8} Because of the low electron temperature and high electron number density, this thickness is small compared to cathode dimensions.

In outline, the mechanism is the following: gas fed through the cathode towards the vacuum region has a product pd (p =pressure, d =interior diameter) which decreases towards the orifice and is essentially negligible at the end. Over a wide range of gas flow rates, the product pd some distance back in the cathode tube is suitable for operation of a high current-density discharge with ionization free-path comparable to the tube size. Also, the fast electrons are trapped in the cavity long enough to produce ionization there. This explains the higher electron density observed in this mode. With this kind of theory Lidsky² concluded that the ratio $\ell:d$ of the length of the cavity to the diameter is important and must be at least 6:1 to permit the electrons which were emitted from the cathode and accelerated through the high electric field of the adjacent sheath to ionize neutral atoms inside the cavity. These ions in turn must collide with the cavity wall with sufficient energy to enhance electron emission. The longer the cavity, and the smaller its diameter, the higher is the probability for ions to collide with the wall before leaving through the orifice.

B. Hollow Cathode Performance Parameters

Although hollow cathodes of various geometries have been operated over a wide range of experimental conditions, it is possible that certain performance parameters remain approximately the same for these conditions. Some parameters which have been evaluated for comparison purposes follow.

1. The current density, j , can be measured at the cathode orifice as

$$j_c = J_i / A_c \quad (\text{II-2})$$

or on the inside surface as

$$j_s = J_i / A_s \quad (\text{II-3})$$

where J_i is the total current from the hollow cathode, A_c is the area of cathode orifice, and A_s is the area of the hollow cathode inside surface. There appears to be a relation between current density and electron emission mechanism.⁴

2. The mean free-path for ionization of the incoming neutrals, λ^i , is^{A-2}

$$\lambda^i = \frac{v_a}{\nu_{ae}^i} = \frac{\text{atom velocity}}{\text{collision frequency for ionization by electrons}} \quad (\text{II-4})$$

$$\lambda^i = \frac{v_a}{n_e(v_e) Q_{ae}^i(v_e) v_e} \quad (\text{II-5})$$

where v_e is the electron velocity and Q_{ae}^i is the ionization cross section. When the denominator is evaluated assuming a linear dependence of the cross section Q on the energy \mathcal{E} (or v_e^2), we get

$$v_{ae}^i = \propto n_{eo} \left(\frac{2}{\pi} \right)^{1/2} \left(\frac{m_e}{kT_e} \right)^{3/2} e^{-\frac{m_e v_t^2}{2kT_e}} \chi$$

$$\left[\left(\frac{2kT_e}{m_e} \right)^3 + \frac{3}{2} v_e^2 \left(\frac{2kT_e}{m_e} \right)^2 + v_e^4 \left(\frac{2kT_e}{m_e} \right) \right] \quad (\text{II-6})$$

where n_{eo} = total electron number density

v_t = velocity where electron energy is at threshold for ionization

\propto = initial slope of the Q versus v_e^2 curve

As has been mentioned, this mean-free-path must be compared to a characteristic length of the cathode cavity, either the length or the diameter, as a ratio K :

$$K_1 = \frac{\lambda^i}{l} \quad (\text{II-7})$$

l : length of the cavity

$$K_2 = \frac{\lambda^i}{d_c} \quad (\text{II-8})$$

d_c : diameter of cavity orifice

An example of a detailed calculation of these different parameters is given in Appendix I.

These parameters have been computed for several hollow cathodes whose operation has been described in references 8,9,17,18,22,23 and 24. The results are summarized in Table I. From the K factors, it is seen that the mean-free-path for ionization is always substantially less than the cavity length, and is usually less than even the cathode orifice diameter.

TABLE I. Comparison of Hollow Cathode Parameters

Ref. No.	J A	d _c mm	j _c A/m ²	j _s A/m ²	m _c mg/sec	n _{eo} m ⁻³	K ₁	K ₂
8	3 to 300	3	4 x 10 ⁵ to 4 x 10 ⁷	4 x 10 ³ to 4 x 10 ⁵	2.5 to 98	1.8 x 10 ²² to 7.3 x 10 ²³	2.4 x 10 ⁻⁴ to 1.2 x 10 ⁻²	≈ 5.6 x 10 ⁻²
9	200	3	2.8 x 10 ⁷	4.2 x 10 ⁵	0.3 to 10	1.8 x 10 ²¹ to 5.9 x 10 ²²	2.1 x 10 ⁻⁴ to 7.0 x 10 ⁻³	10 ⁻² to 0.32
17	0.5	0.13 to 0.5	2.5 x 10 ⁶ to 4 x 10 ⁷	1.3 x 10 ³	2 x 10 ⁻² to 0.7	1.4 x 10 ²² to 5 x 10 ²³	6.6 x 10 ⁻⁵ to 2.3 x 10 ⁻⁵	3 x 10 ⁻³ to 10 ⁻¹
18	0.25	0.08 to 0.3	4 x 10 ⁶ to 5.5 x 10 ⁷	6.8 x 10 ⁴	3.2 x 10 ⁻² to 5.3 x 10 ⁻²	1.5 x 10 ²² to 3.5 x 10 ²³	6.8 x 10 ⁻⁴ to 1.6 x 10 ⁻²	5.8 x 10 ⁻² to 1.3
22	500 to 600	11	3.2 x 10 ⁶ to 6.3 x 10 ⁶	2.3 x 10 ⁵ to 4.7 x 10 ⁵	5 to 90	10 ²² to 1.7 x 10 ²³		
23-24	0.3 to 3.0	≈ 0.2	10 ⁷ to 10 ⁸	8.2 x 10 ⁴ to 8.2 x 10 ⁵	4.2 x 10 ⁻² to 0.3	2.1 x 10 ²³ to 1.7 x 10 ²⁴	1.3 x 10 ⁻⁴ to 1.1 x 10 ⁻³	1.2 x 10 ⁻² to 10 ⁻¹

C. Criteria for Hollow Cathode Operation

Three criteria must be satisfied to guarantee proper hollow cathode operation. The first requirement in a low current cathode is sufficient thermionic emission. This emission is produced by heating the cathode to approximately 1500 °K (for a tungsten cathode). In the hollow cathodes of ion thrusters, electron emission is enhanced at this low temperature by the presence of BaO on the insert, due to the resulting low work functions. In the case of quasi-steady MPD arcs, the heating of the cathode surface has to be due to the deposition of energy by the discharge itself, enhancing the electron emission by a cumulative effect. This process may be explained as follows: during the breakdown phase the initial positive ions acquire enough energy in the electric field to cause emission of some electrons when they collide with the inside cathode wall. Now a potential sheath will form on the cathode, with two main consequences.

1. Electrons can be extracted from the cathode by field emission.
2. Ion bombardment energies now increase enough to heat the cathode sufficiently to emit electrons thermionically. Once this regime is reached, one can say that the discharge is in a quasi-steady mode.

The second requirement is an accelerating field for the electrons, provided by a large enough potential difference. To start a discharge, one has to extract electrons from the cathode. An accelerating field is necessary to give the electrons high enough energy, so that when they collide with neutrals they ionize them.

The third requirement is a sufficiently high neutral gas density to supply the necessary current carriers. It can already be pointed out that because of this requirement the mass flow is going to play a very important role.^{18,27}

CHAPTER III. STUDY OF HOLLOW CATHODE MPD DISCHARGE

A. Apparatus and Hollow Cathode Design

Apparatus

Argon propellant is injected into the discharge chamber through a solenoid valve and multi-tube manifold to six 0.48-cm injectors, and also through the hollow cathode orifice, in the configuration shown in Fig. 1. The mass flow rate is controlled by the argon reservoir pressure, and the tube length to the gas-triggered switch is so chosen that the discharge in the main chamber takes place during the period of constant mass flow. Power is supplied as an essentially rectangular current pulse from a 3000- μ fd, high-voltage capacitor line or, alternatively by a 96,000- μ fd electrolytic capacitor bank. The current is monitored by a Rogowski loop around the cathode lead and the terminal voltage is measured with a Tektronix P-6013A probe. All data are recorded on a Tektronix dual beam oscilloscope.

In addition to these parameters normally used to describe arc operation, namely discharge voltage, discharge current and total mass flow, an important new parameter has been added for the hollow cathode - the fraction of the total mass flow that goes through the cathode cavity. It has already been found in previous work done on the MPD device,^{A-3} that for proper operation at any given current, the discharge needs a certain mass flow. If this mass flow is not provided, the so-called starved condition prevails and the discharge will feed itself by taking mass from somewhere else, such as ablation of insulators and even the electrodes.

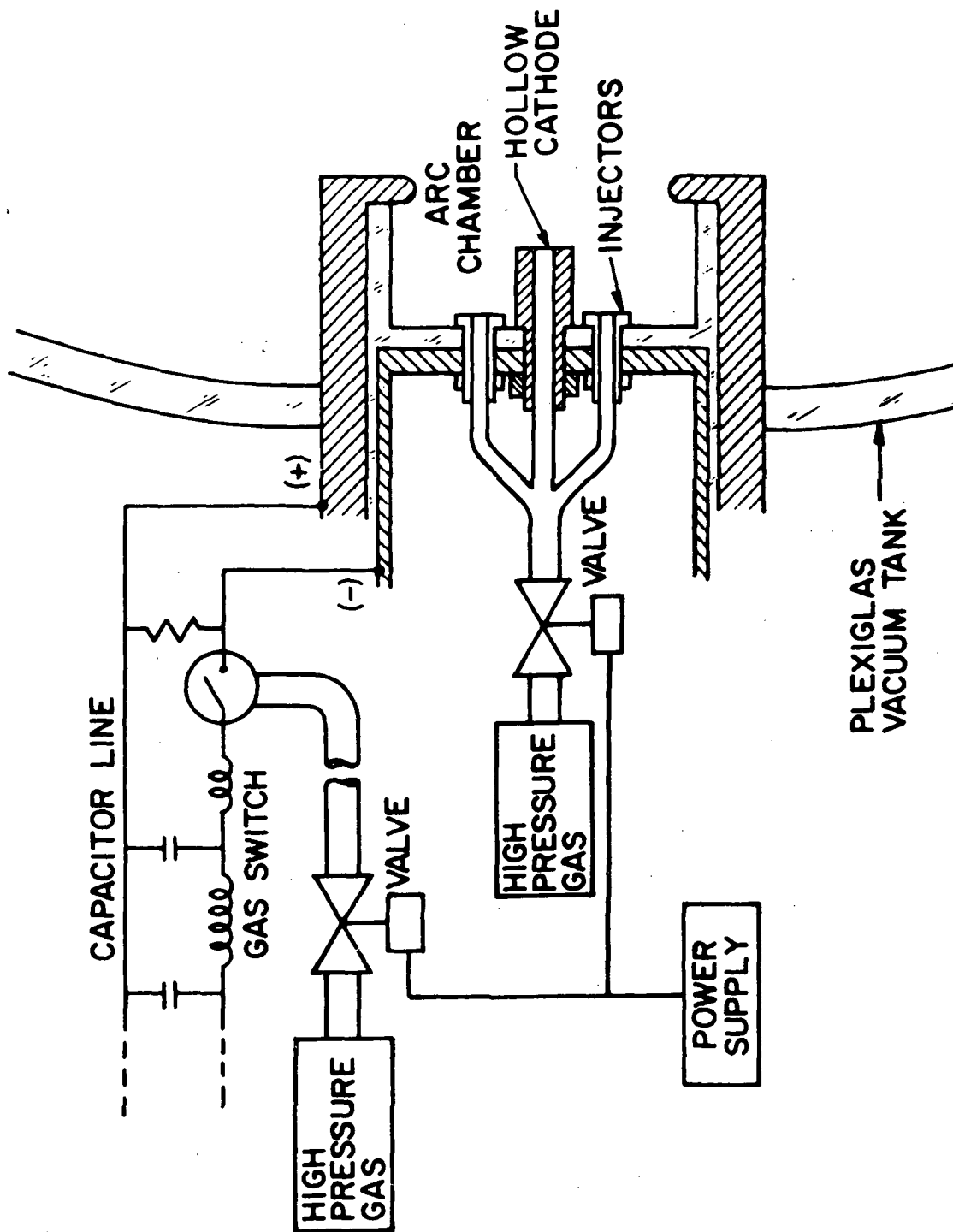


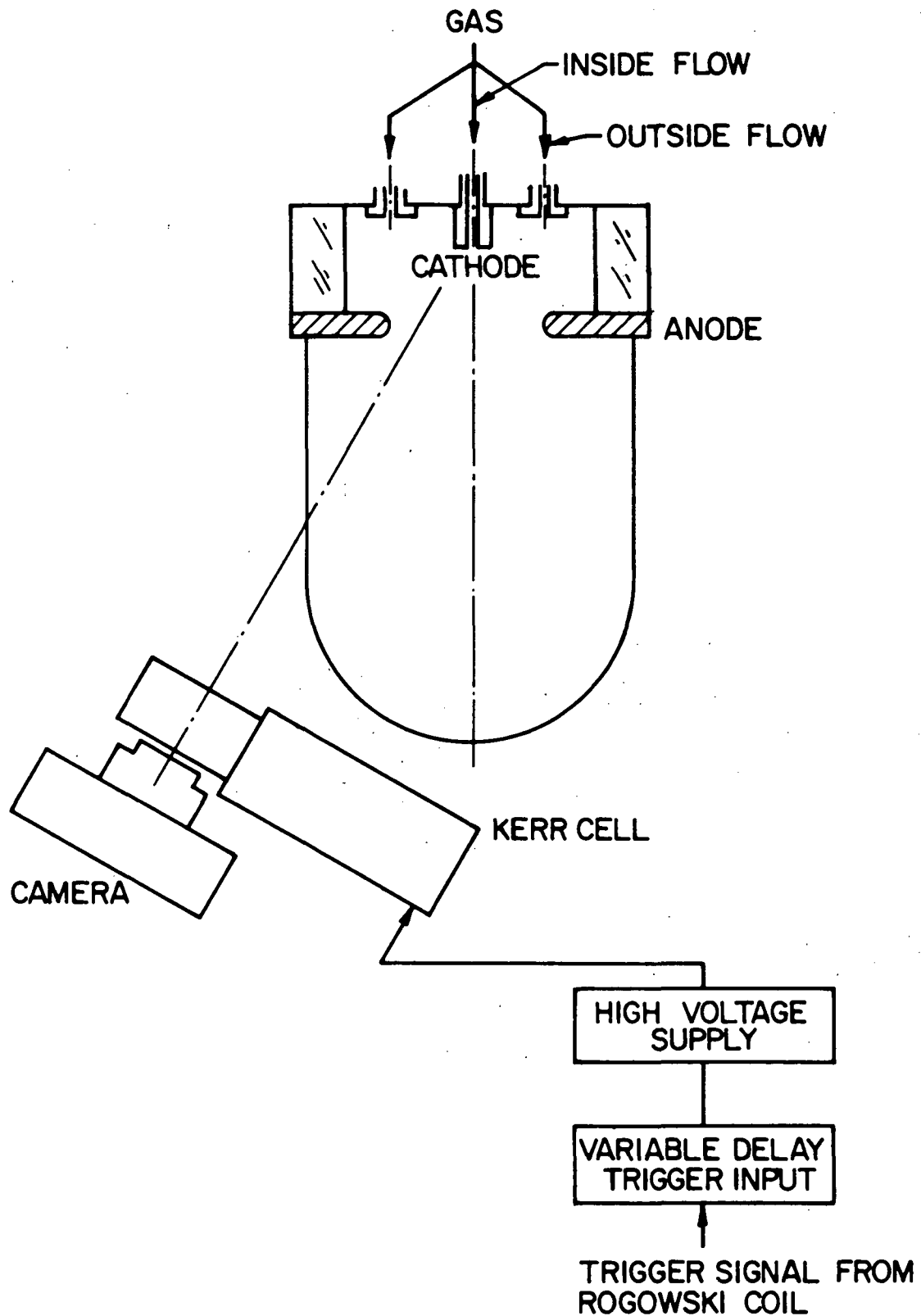
FIGURE 1
AP 25 R 4681 71

HOLLOW CATHODE EXPERIMENTAL CONFIGURATION

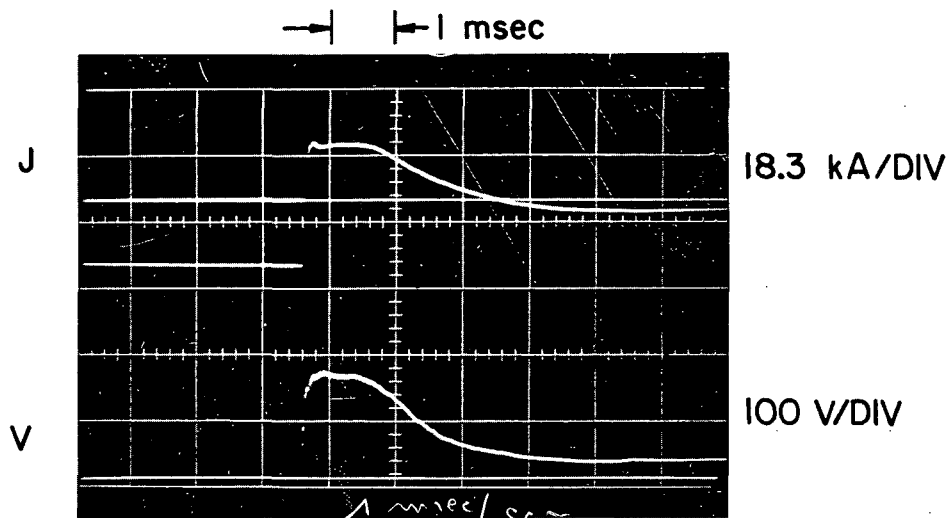
For the current attachment to be distributed over the entire surface of the hollow cathode, a particular mass flow may be required both inside the cavity and outside it in the chamber. For this reason, the mass injection system was constructed to allow variation of the fraction of the total mass flow which is admitted through the cathode "inside". Practically this was done by putting plugs with different orifices into the injection tubes. Cold flow tests revealed that the inlet flow was choked at the solenoid valve and not at these restrictions in the injection tubes. This allowed convenient setting of the total mass flow by the reservoir pressure, but prohibited scaling the fractional flow division with the ratio of inside to outside injection areas. Therefore, an experimental calibration was necessary. This was done by opening the solenoid valve for a certain time, and trapping the gas that flowed outside and inside the cavity of the cathode in two different vacuum vessels. By measuring the pressure rise in these vessels, an exact measurement of the flow division could be made.

Steady mass flow was indicated when the output of a fast ionization gauge put in front of the injectors was constant. This probe essentially measures particle density, but one can assume that the mass flow is steady when the number density as a function of time attains a plateau. This point is normally reached 3 msec after opening the valve.

Pictures of the discharge were also taken through a 5 μ sec Kerr-cell shutter. The experimental set-up for this is shown in Fig. 2. By delaying the trigger signal for various increments, photographs of the discharge could be taken during the initial transient or at any time during the steady phase. A typical record of current and voltage for the electrolytic capacitor bank is shown in Fig. 3.



ARRANGEMENT FOR KERR-CELL PHOTOGRAPHY



TYPICAL CURRENT AND VOLTAGE RECORD
ELECTROLYTIC BANK

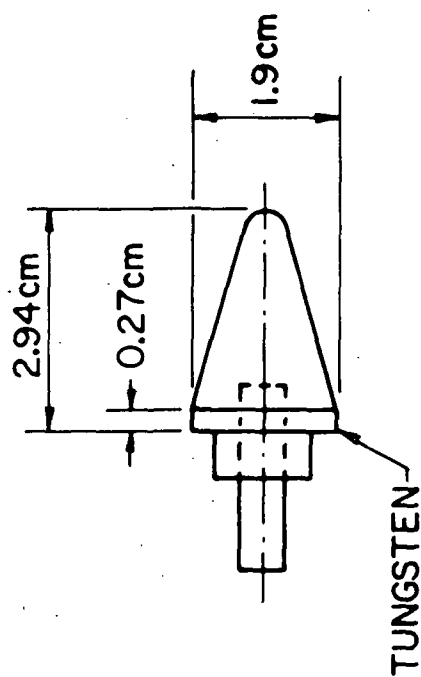
All tests were performed with the arc chamber attached to a 22.8-cm-diam by 45.7-cm-long Pyrex bell jar evacuated by a 7.1- ℓ /sec vacuum pump. The average pressure reached in the bell jar before each shot was approximately 5 μ .

Design

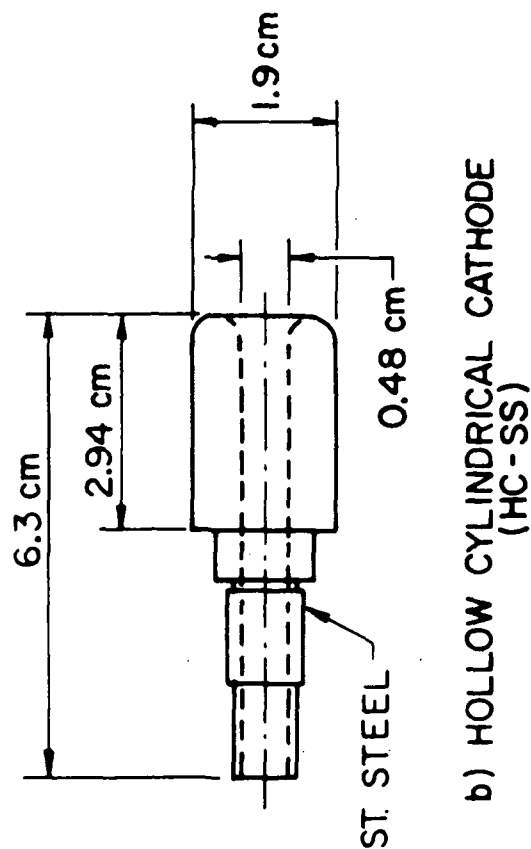
To change the original configuration as little as possible, the first hollow cathode geometry was made cylindrical, of diameter equal to the maximum diameter of the standard solid conical cathode, and also the same length, Figs. 4a and b. (For simplification throughout the text, the hollow cathodes will be given an abbreviated designation. The stainless steel cylindrical hollow cathode discussed here bears the notation HC-SS.) The inside diameter was chosen as a compromise so that the ℓ/d ratio, already mentioned before,² is as close as possible to 6. For the first measurements stainless steel, instead of tungsten was used for convenience.

Next we tried to find a possible mechanism to force the discharge inside the hollow cathode. Previous measurements with the conical cathode showed that the current density is approximately uniform over the cathode surface. Assuming a similar uniform distribution exists for the hollow cathode, the current lines can be estimated for this case (Fig. 5). This figure shows that the current lines have the opposite radial direction inside and outside. Since the magnetic field has the same azimuthal direction inside and outside, the cross-product $\hat{j} \times \hat{B}$ of current density and magnetic field yields an upstream force in the cavity, compared with the normal accelerating downstream force outside. The force per unit area, or magnetic pressure is equal to

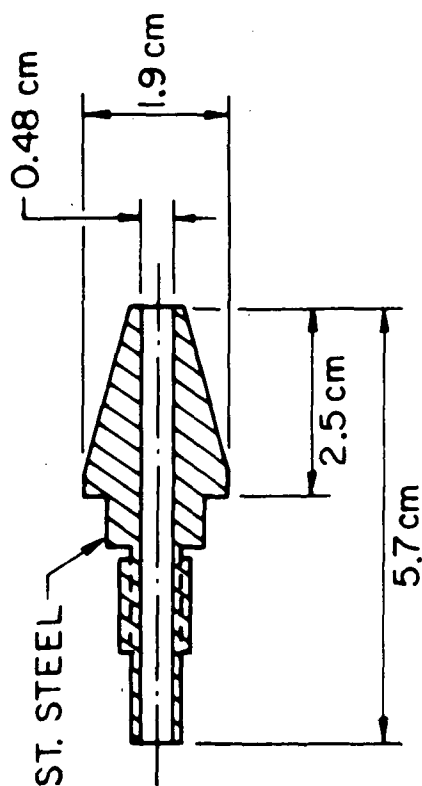
$$\frac{B^2}{2\mu_0}$$



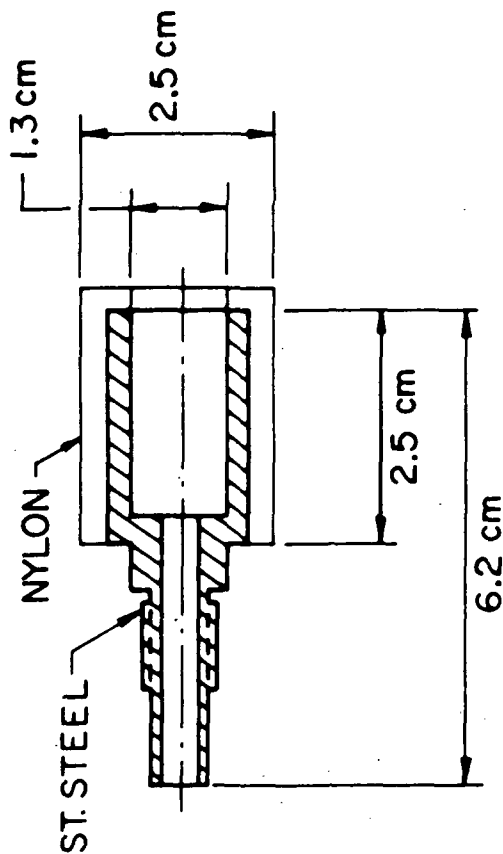
a) SOLID CONICAL CATHODE



b) HOLLOW CYLINDRICAL CATHODE
(HC-SS)

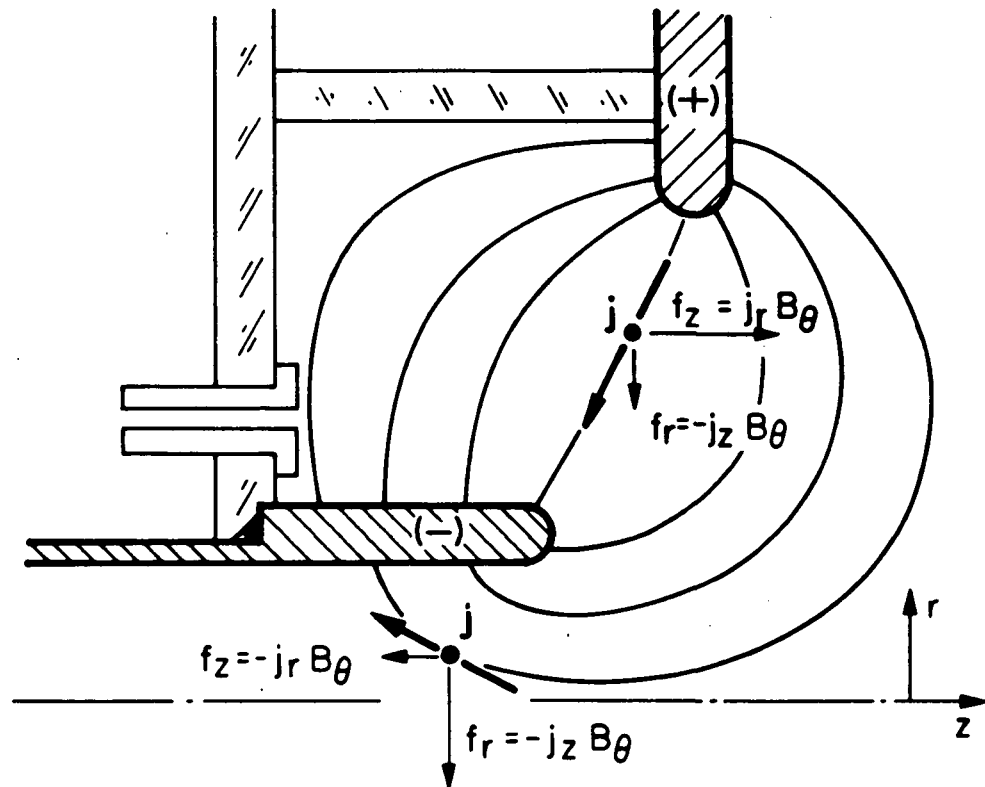


c) HOLLOW CONICAL CATHODE
(HC-CON)



d) INSULATED HOLLOW CATHODE
(HC-INS)

CATHODE CONFIGURATIONS



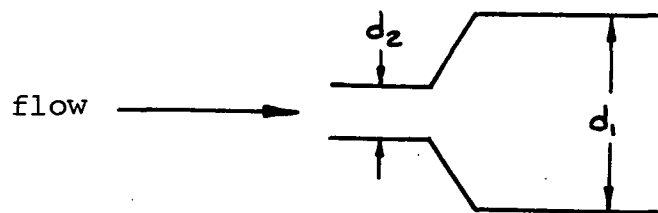
HOLLOW CATHODE CURRENT PATTERN

where B is the magnetic field and μ_0 the permeability of free space. To get a large magnetic pressure, a high current density is required at the cathode tip. This was obtained by boring a 0.48-cm-diam hole in a solid conical cathode, as shown in Fig. 4c. This cathode (HC-CON) thus has a sharp corner, where the current prefers to attach. Once the discharge is started, the magnetic pressure should tend to push it inside.

A concentrated study of the literature on hollow cathodes was made in order to have a theoretical basis for further design changes. The basic information for the design of later hollow cathodes was found in NASA report CR-72891 "Cathode Studies of a Radiation Cooled MPD Arc Thruster," done by McDonnell-Douglas from which the main points are summarized here.

- Arc voltage increased, and consequently higher input power could be achieved, with smaller electrode gaps.
- Stable operation was achieved after some initial instability by lowering the propellant flow rate. The arc attachment was observed to move from the outside diameter into the hollow section of the cathode. When this arc movement occurred, the exhaust narrowed into a tight beam.
- A decrease in voltage was observed with increasing hollow cathode cavity diameter, for the same current, or for the same voltage a higher current.
- Efforts to increase arc voltage by changing the methods of gas injection proved to be unsuccessful.
- An alternative means of increasing the voltage was to increase the anode throat diameter.

- For a cathode with a flat front face (the previous ones were conical), the arc-attachment tended to shift to the outside diameter of the cathode as the current was increased. A reduction of the current usually allowed re-attachment of the discharge in the cathode cavity.
- A 10° inverted conical face rather than the flat one of the previous cathode improved the cathode attachment stability significantly and resulted in operation over a wider range of mass flow rates than earlier ones.
- Addition of propellant flow around the hollow cathode usually caused the arc attachment to move from the cavity to the outside diameter of the cathode.
- Argon is an acceptable propellant for cathode attachment stability.
- It became apparent that improvements in performance and reliability were closely related to the location of arc attachment.
- For a current range of 150 to 700 A and an external magnetic field of 0.15 Tesla, the plume mode, or high voltage mode, is characterized by current attachment on the tip, whereas the low voltage mode or spot mode is characterized by current attachment near the inner base.
- If the mass flow was increased, the external magnetic field had to be decreased in order to keep a stable discharge inside.
- The ratio of the inside diameter over the connection diameter d_1/d_2



has to exceed a certain minimum of approximately 2 for a stable discharge.

In the facilities which we are using in Princeton, there is no external heat addition to the hollow cathode. So, if we are in a regime where thermionic emission is possible, the only way to get the necessary temperature is by self-heating. The location of the maximum self-heating is deduced to be the region of the cathode tip, from visual inspection of used cathodes. To avoid the temperature gradients produced by self-heating, the walls have to be made thicker.⁴ This same reference also notes for $j \approx 10^3$ A/cm² thermionic emission is important, whereas for $j \approx 10^4$ - 10^5 A/cm² both field and thermionic electron emission are important. Having field emission too, there must be a rather large voltage drop to extract these electrons. Ions are coming into this voltage fall, with the result that they get enough energy to bombard the cathode causing erosion. There are indications that the wear is less when the orifice diameter is decreased and tip thickness is increased.²⁷

Concerning the cavity length, reference 4 shows that the tip temperature decreases with the length of the cathode for the same current, and also the longer, the more uniform the current will be distributed over the inside surface. Also for the same current, as the length is decreased, it is observed that the inside surface electric field increases. A higher field inside may encourage the more productive emission mechanisms.

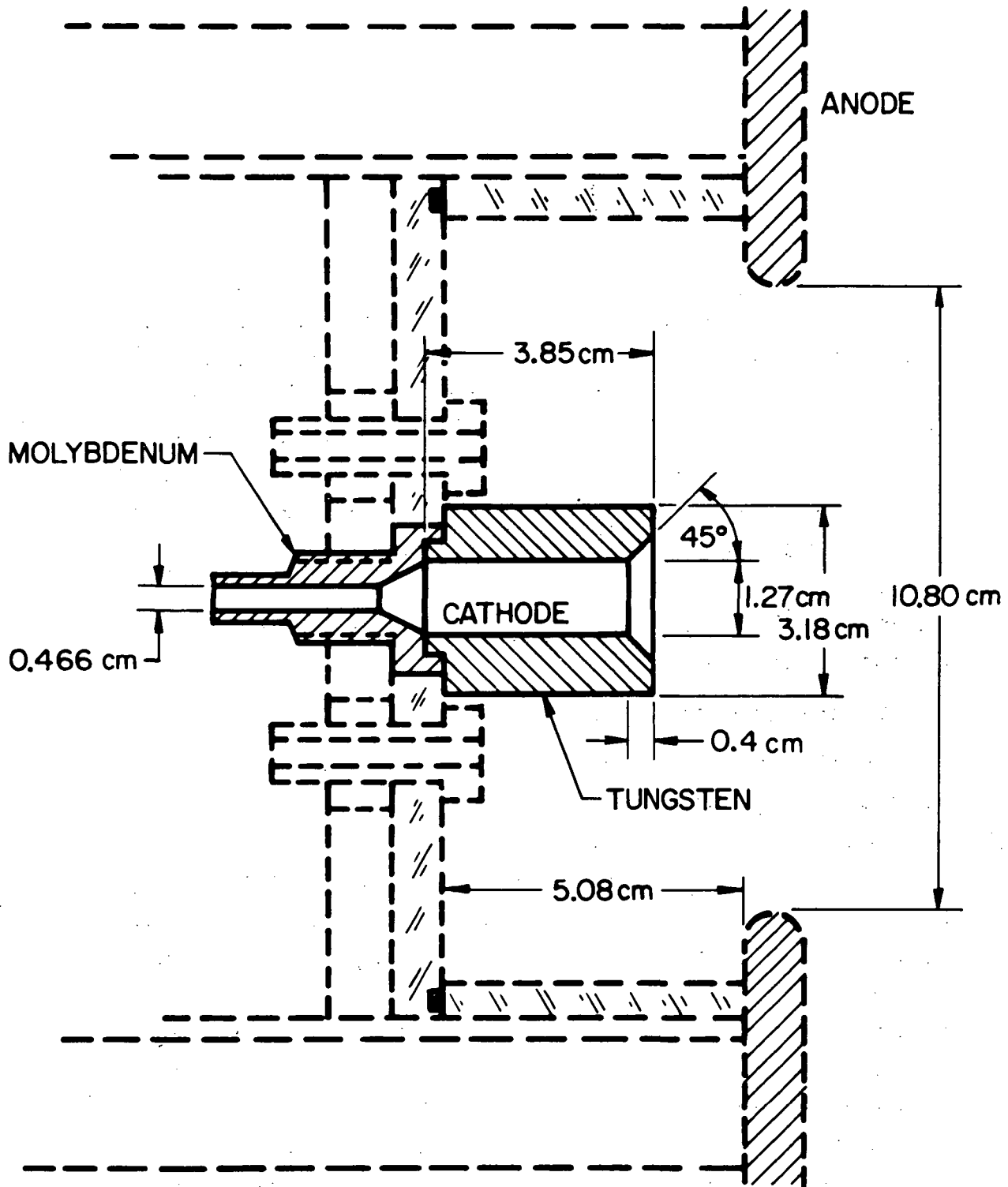
With this information and other practical considerations in mind, the following two cathode geometries were tried. The first is the insulated cylindrical hollow cathode (HC-INS) shown in Fig. 4d. Because the total discharge current of some tens of kA must pass through the cathode orifice, this diameter was increased from 0.48 cm to 1.27 cm. This large diameter might also encourage deeper penetration of equipotentials, thus creating a higher surface electric field. In an attempt to force the current to attach on the inside of the cavity, the outside surface was covered with nylon, but this proved unacceptable because of severe erosion

of the nylon; after about 50 shots of 1 msec duration, the front insulation had completely disappeared. It is possible that this ablation influences the data for this cathode, especially in the region where the discharge is starved.

Previous hollow cathodes were made out of stainless steel. In our pulsed MPD accelerator, the current density is sufficiently high that field emission must supplement the thermionic emission. The rate of this electron field emission is primarily related to the work function of the material. Thus the work function could be as important a factor as the geometry. Therefore the final hollow cathode was made of tungsten. The dimensions and shape are based on all the information given before. The back piece of this hollow cathode was made out of molybdenum, due to brittleness and manufacturing problems of tungsten, and also because of costs. The tungsten cylindrical hollow cathode (HC-W) is shown in Fig. 6, together with the exact geometry of the discharge chamber.

B. Discharge Characteristics

Before operating with the hollow cathode, voltage-current discharge characteristics were taken with the solid conical tungsten cathode for comparison, at several different mass flow rates. Cylindrical hollow cathode experiments (HC-SS) were then conducted for various total mass flows, and differing ratios of mass flows through the outer injectors and cathode cavity. Figure 7 displays the characteristics for 6 g/sec total mass flow, in comparison to solid cathode operation in the same regime. The main points to be noted are that for one mass flow combination e.g., 14% of the total flow passing through the cathode, the hollow cathode displays a substantially lower impedance than the solid cathode version. For other ratios, however, this comparison is reversed, thus indicating both a potential reduction of cathode losses by hollow cathode techniques, and a sensitivity of this benefit to mass flow distribution.



TUNGSTEN HOLLOW CATHODE (HC - W)
AND DISCHARGE CHAMBER GEOMETRY

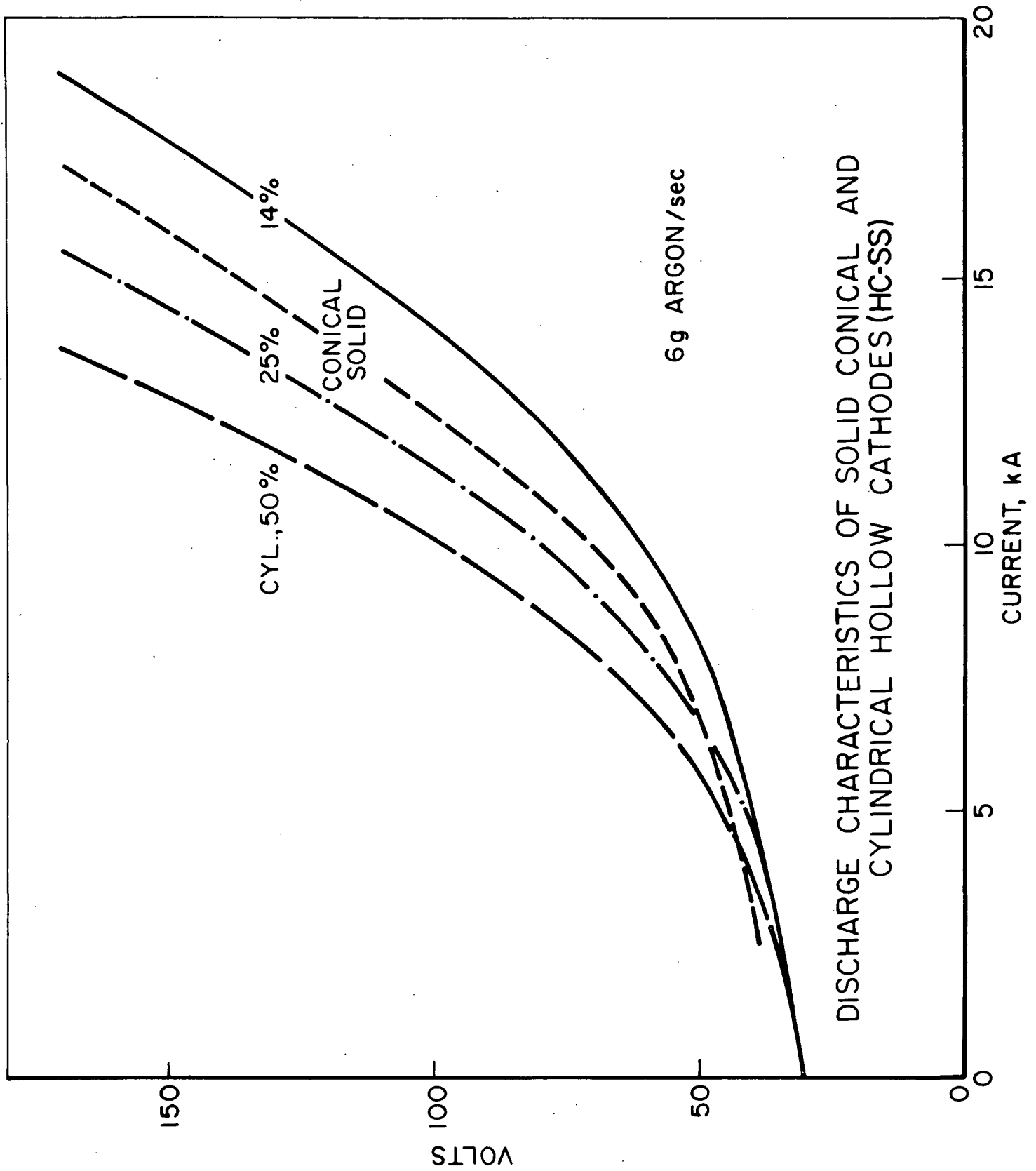


FIGURE 7
AP 25 4700 71

To pursue this point further, Fig. 8 shows a comparison of characteristics for total mass flows of 3, 6 and 10.5 g/sec, all with 14% of the total flow through the cathode. Clearly indicated is a sensitivity to the absolute value of the flow through the cathode, as well as the ratio, suggesting that a full survey of all reasonable permutations is necessary to identify the optimum operating conditions.

Even more distinct differences were obtained with the tungsten cylindrical hollow cathode (HC-W). Typical HC-W discharge characteristics for different total mass flows and combinations of mass flow through the outer injectors and cathode cavity are shown in Fig. 9. On the vertical axis we have the discharge voltage and on the horizontal axis the discharge current. Lines of constant mass flow have been drawn for mass flows of 3, 5.4, 7.9 and 10.5 g/sec for both 20% and 100% of the mass flow inside. It is remarkable that for 20% inside, the discharge characteristics are quite spread out, whereas for 100% there is almost no mass flow influence at all.

It is of interest to compare the HC-W with the solid conical cathode in the same regime of operation. Note that for the HC-W the voltage increases with increasing mass flow, whereas for the tungsten solid conical cathode, Figure 10, the voltage decreases for increasing total mass flow. This difference was also found for zero mass flow through the hollow cathode. This means that the very existence of a cavity in the cathode causes a drastic change in operation. In other words, the geometry of the cathode is a very important parameter.

Since we have a combination of mass flow outside and inside, there are the possibilities that only the gas flow outside, or inside, or both together determine the discharge phenomena. Figure 11 shows the results of tests to determine whether just the inside or just the outside flow dominates the discharge impedance characteristics. Here we have the characteristic for a total mass flow of 5.4 g/sec of which 45% is

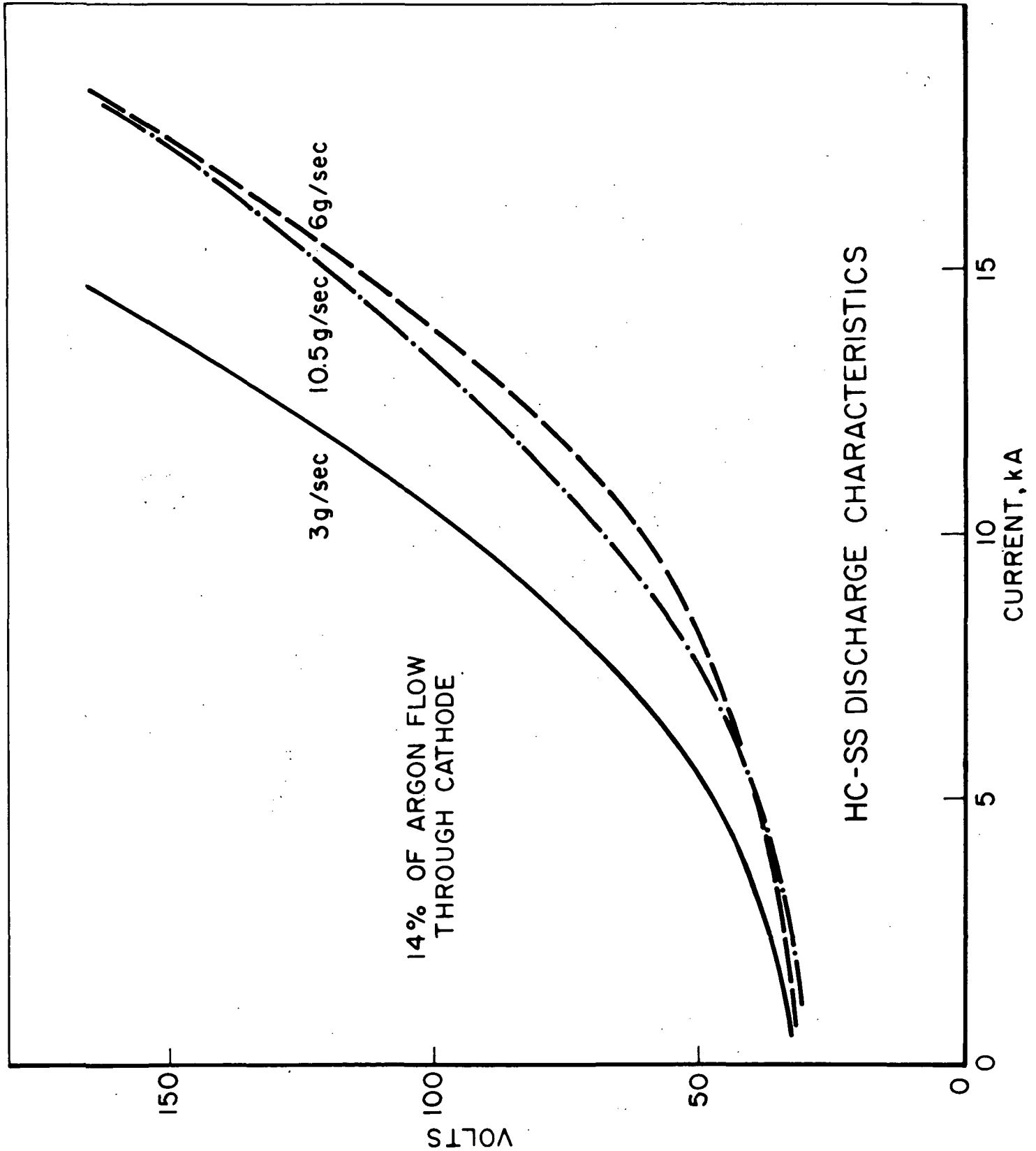
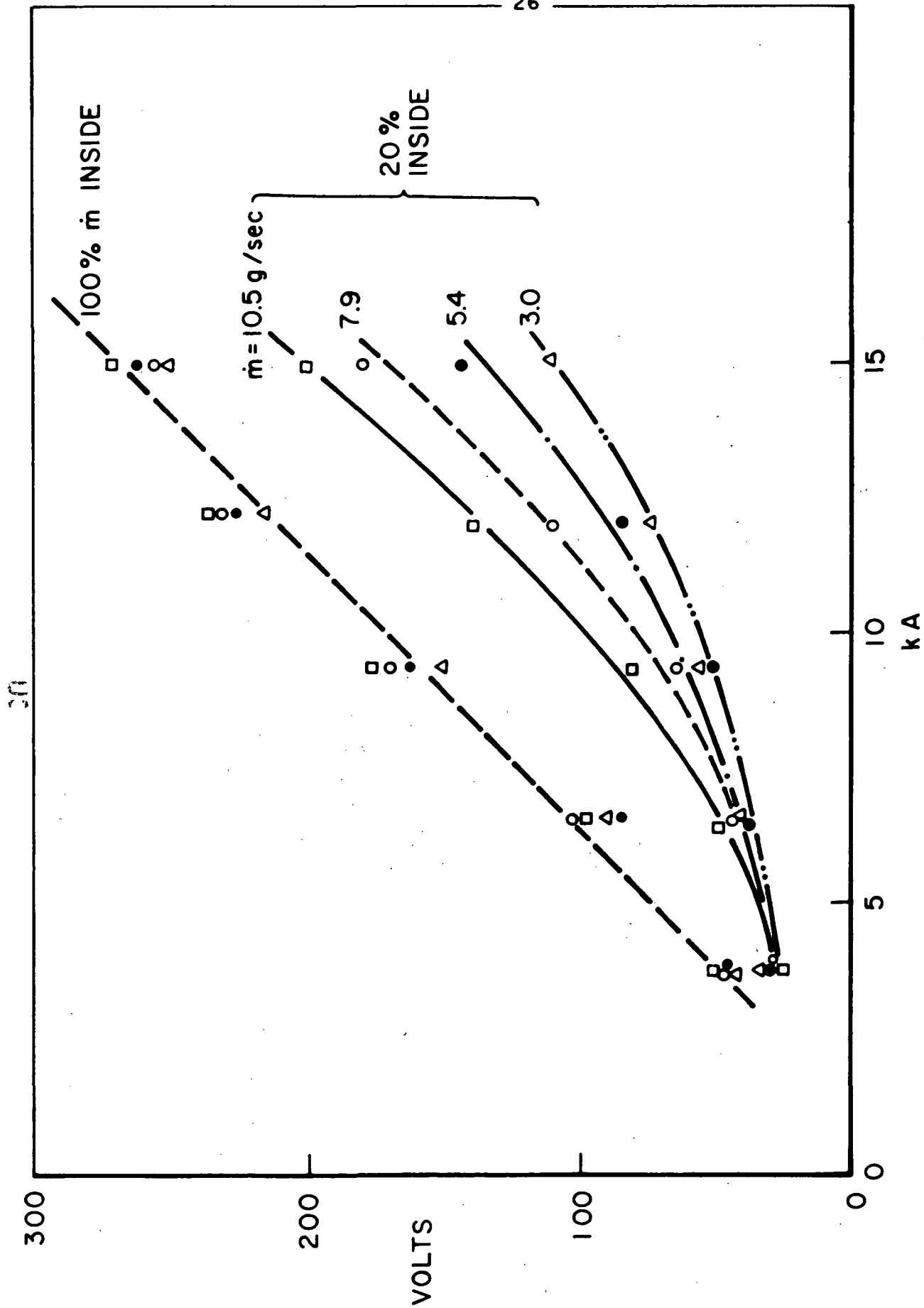


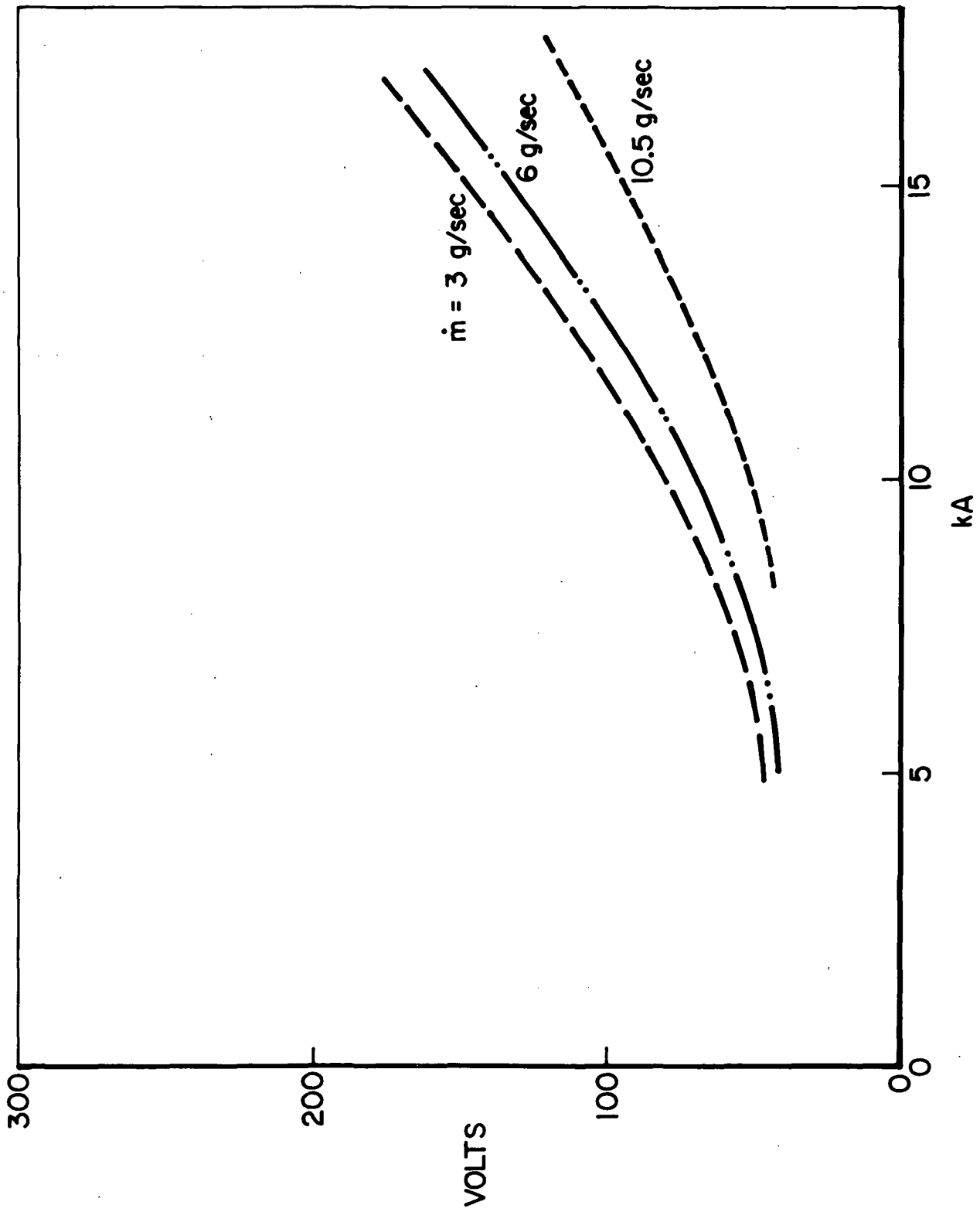
FIGURE 8
AP 25 4702 71



HC-W CHARACTERISTICS

FIGURE 9

AP25, 4772 71



TUNGSTEN SOLID CONICAL CATHODE CHARACTERISTICS

FIGURE 10
AP 25 4771 71

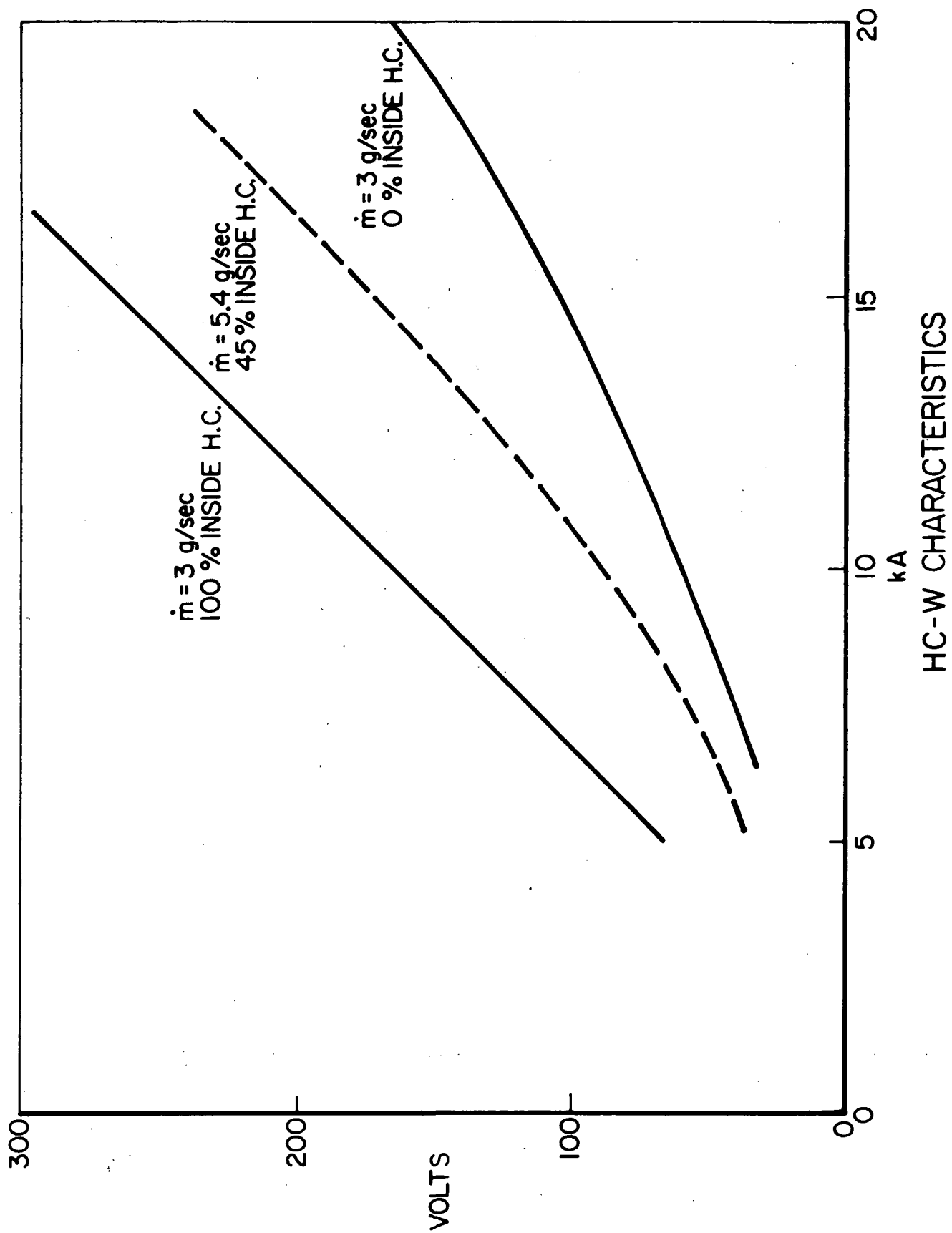


FIGURE II
AP 25 4774 71

inside, i.e., 2.45 g/sec inside, and 2.95 g/sec outside. If the mass flow inside does not participate at all in the discharge, the characteristic of 5.4 g/sec total (2.95 g/sec outside) should agree with the 3 g/sec outside, zero flow inside case. That it does not implies that the hollow cathode mass flow has an effect on the discharge. A similar comparison between the 5.4 g/sec characteristic and the 3 g/sec inside, zero flow outside case reveals that the hollow cathode does not completely dominate the characteristic. Thus, we can conclude that both mass flows outside and inside determine the specific operation of the hollow cathode discharge.

It is stated in the literature^{18,23,24} that proper operation of a hollow cathode in low power regimes (5 kW) is accompanied by a low discharge voltage and higher current compared to the standard solid cathode. To check this with the HC-SS in a power region of 0.5 to 2.5 MW, the voltage was monitored for a fixed current and mass flow as the flow percentage inside was increased. Results of this are shown in Fig. 12. Here we have the discharge voltage on the ordinate and the fraction of the flow inside on the abscissa, with current as a parameter. This graph tells us that the voltage increases with increasing inside flow. If low voltage alone were the indication of proper operation of a hollow cathode, this figure would indicate a preference for zero percent of the mass flow inside, but this conclusion is bothersome for two reasons. First, in the lower power case, proper hollow cathode operation was only observed when non-zero mass flow was passed through the cathode. Second, photographs of the discharge, taken during the steady phase, Figure 13, indicate that for no cathode flow the discharge luminosity consists of an overall shroud over most of the exterior surface, suggesting that hollow cathode function had not been achieved. For 20% of the mass flow inside, there is a jet of plasma coming from the tip and center of the hollow cathode. These observations place in considerable doubt the contention that the lowest voltage in Fig. 12 is an indication of proper hollow cathode operation.

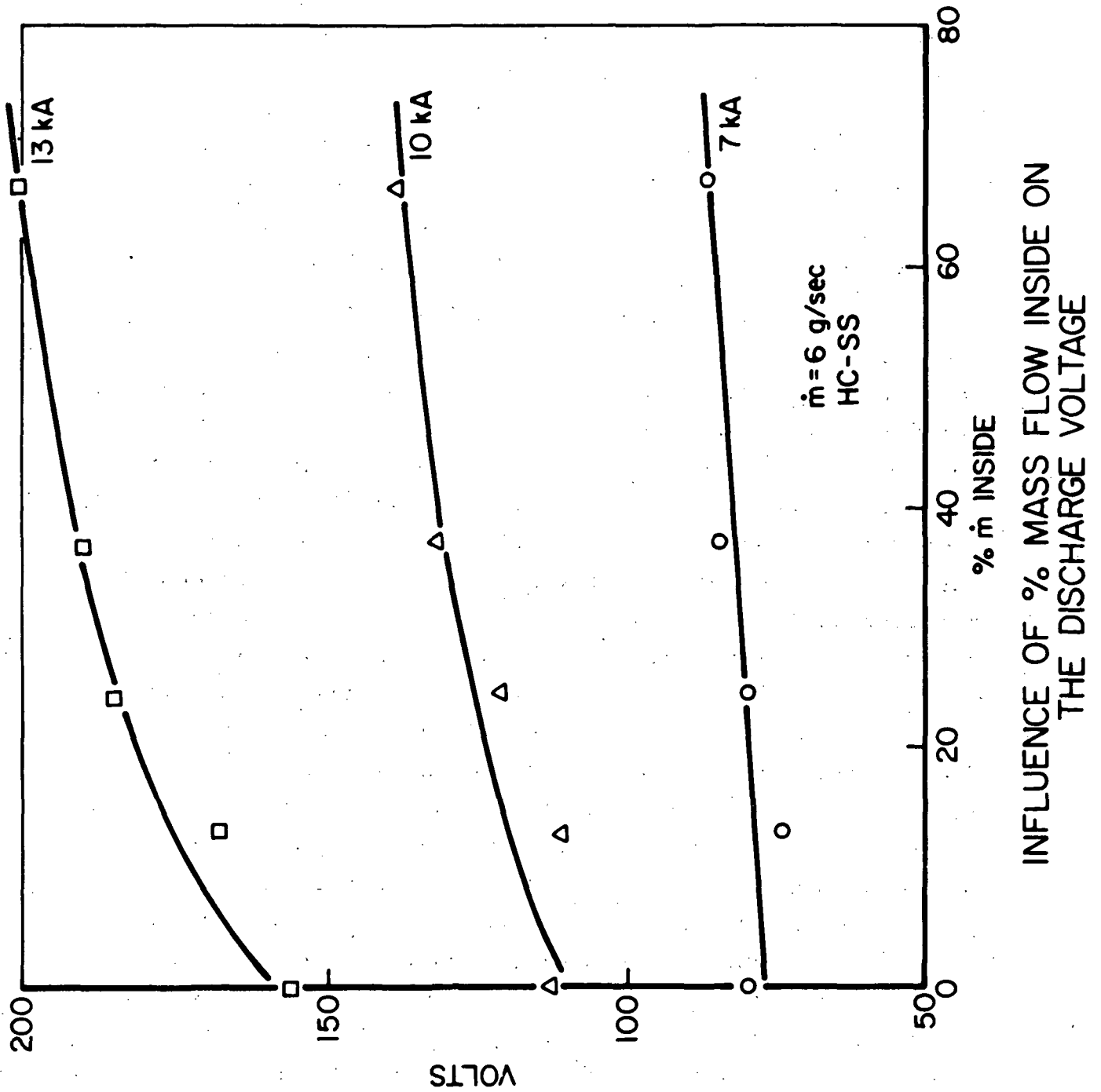
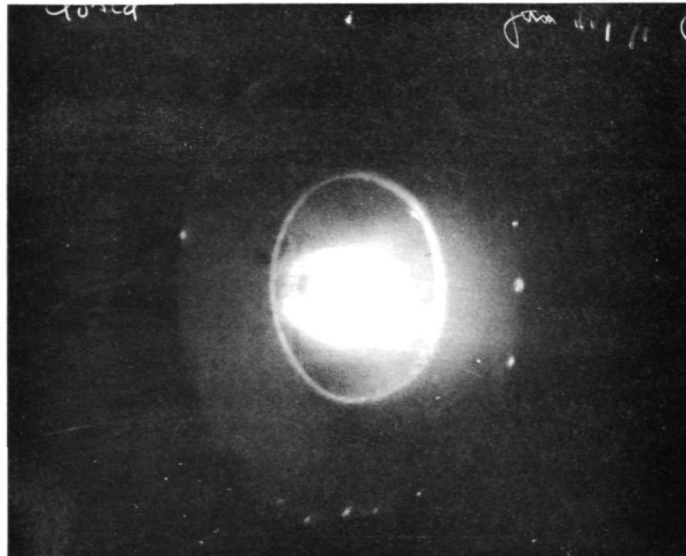
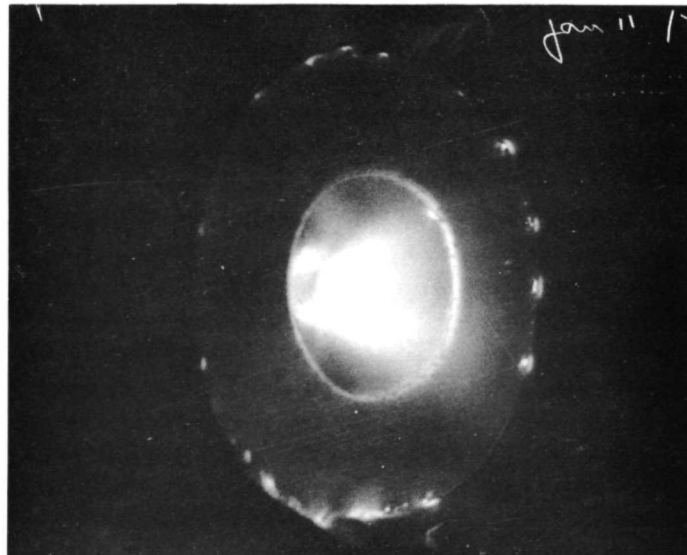


FIGURE 12
AP25 4797 71



a) 90 V \times 11.9 kA
6 g/sec ARGON
NO CATHODE FLOW



b) 95 V \times 13.5 kA
6 g/sec ARGON
20 % THROUGH CATHODE

HC - SS DISCHARGE

Data in Fig. 12 may instead be dominated by an additional effect. Earlier experiments with floating potential probes have shown both an increase in the anode voltage drop and its extension toward the discharge centerline as the mass flow is decreased at a given current level.^{A-3} It is reasonable to interpret this growth toward the region of greater electron number density as the mechanism for providing the additional current carriers necessary to conduct the total current to the anode. This "anode effect", which manifests itself as an increase in total discharge voltage, may prevail for the data in Fig. 12 since, as the fractional mass flow through the cathode is increased, thereby decreasing the chamber mass flow, fewer charge carriers are available near the anode. Evidence that this effect may become dominant for the hollow cathode is found for the extreme case of 100% of the mass flow inside; for that condition, no discharge occurs.

There are several ways to improve this situation and thus prevent the anode effect from dominating the characteristics of the hollow cathode. One way is to put the anode farther downstream, as suggested by the experiments of reference 38 that the farther downstream the anode, the lower the discharge voltage, and further indicated by the spectroscopic observation that the region of highest electron density in front of the solid conical cathode MPD arc expands radially in the downstream direction.^{A-4} Another improvement that could be made is to increase the cavity orifice diameter as mentioned previously and as reinforced in reference 38, even though this may reduce the net thrust somewhat.^{A-1}

Since we chose to retain the overall chamber dimensions, the latter course was taken. The success of this increase in diameter is proved by the discharge characteristics of the HC-INS, which has an inside diameter increased from 0.48 cm to 1.27 cm. These characteristics are taken for different percent mass flow inside, but all for the same total mass flow of 2.1 g/sec. The results are summarized in a graph with voltage on the vertical axis, fraction of the flow inside on

the horizontal axis, and current as a parameter (Fig. 14). There seems to be a general tendency for increasing voltage with increasing fraction of the flow inside for the high current case because of the "anode effect" described previously, but above 50% of the mass flow through the cathode, the voltage decreases with increasing flow fraction inside for the low current regimes, indicating the hollow cathode effect, as is the case for low power hollow cathodes.

Changing the total mass flow but keeping a fixed terminal discharge voltage gives us more information on the influence of the two main parameters - mass flow and fraction of mass flow inside. Several tests were conducted for constant percent inside while changing the total mass flow. A typical result is shown in Fig. 15. Note the appearance of a maximum current for a particular mass flow. As this optimum is not distinct, a more sensitive Rogowski coil was installed, but with the same reproducible results. Similar graphs for different fractional flows inside were made, and they all show a similar optimum.

These trends are summarized in Fig. 16, where the mass flow is plotted against the fractional division of the flow for several values of current and a fixed terminal voltage of 220 volts. For a fixed percentage flow inside, the data indicate that there are two different injected flow rates where the power input into the discharge is the same. Stated another way, there is an optimum mass flow rate (defined as the maximum current for a fixed voltage) for any given distribution of the flow between outer injectors and the cathode. The locus of these optimum mass flows coincides with a line of constant ratio J^2/\dot{m} , the constant equal to $75 \text{ kA}^2\text{-sec-g}^{-1}$ for these particular data.

The significance of this parameter J^2/\dot{m} is presented by Malliaris^{A-5} and is briefly summarized here.

- Neither of the 2 variables J or \dot{m} is individually limited in any detectable sense. However, experimental evidence indicates that the ratio J^2/\dot{m} appears to have

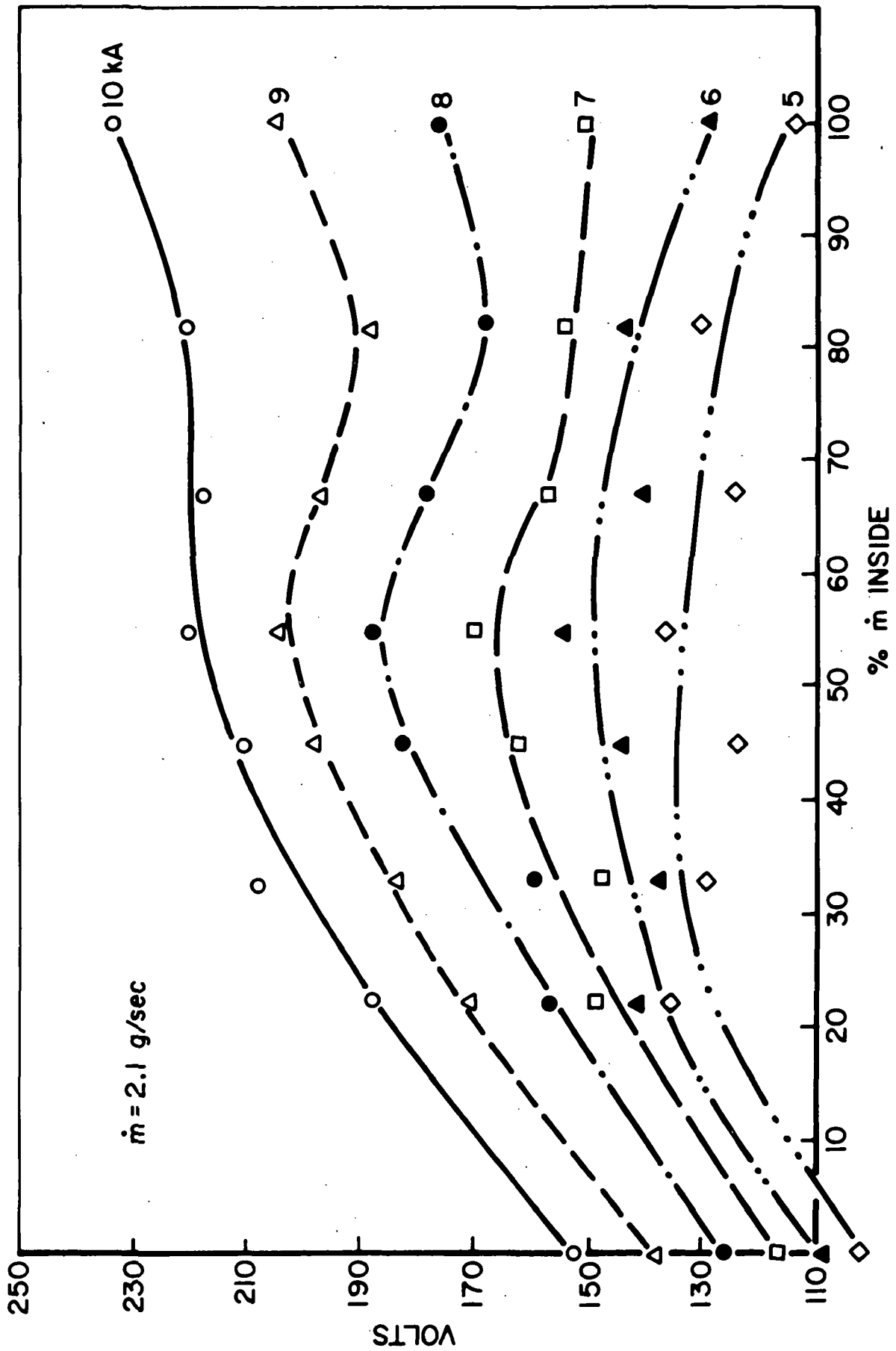


FIGURE 14
AP25 4726 71

SUMMARY OF DISCHARGE CHARACTERISTICS OF INSULATED HOLLOW CATHODE

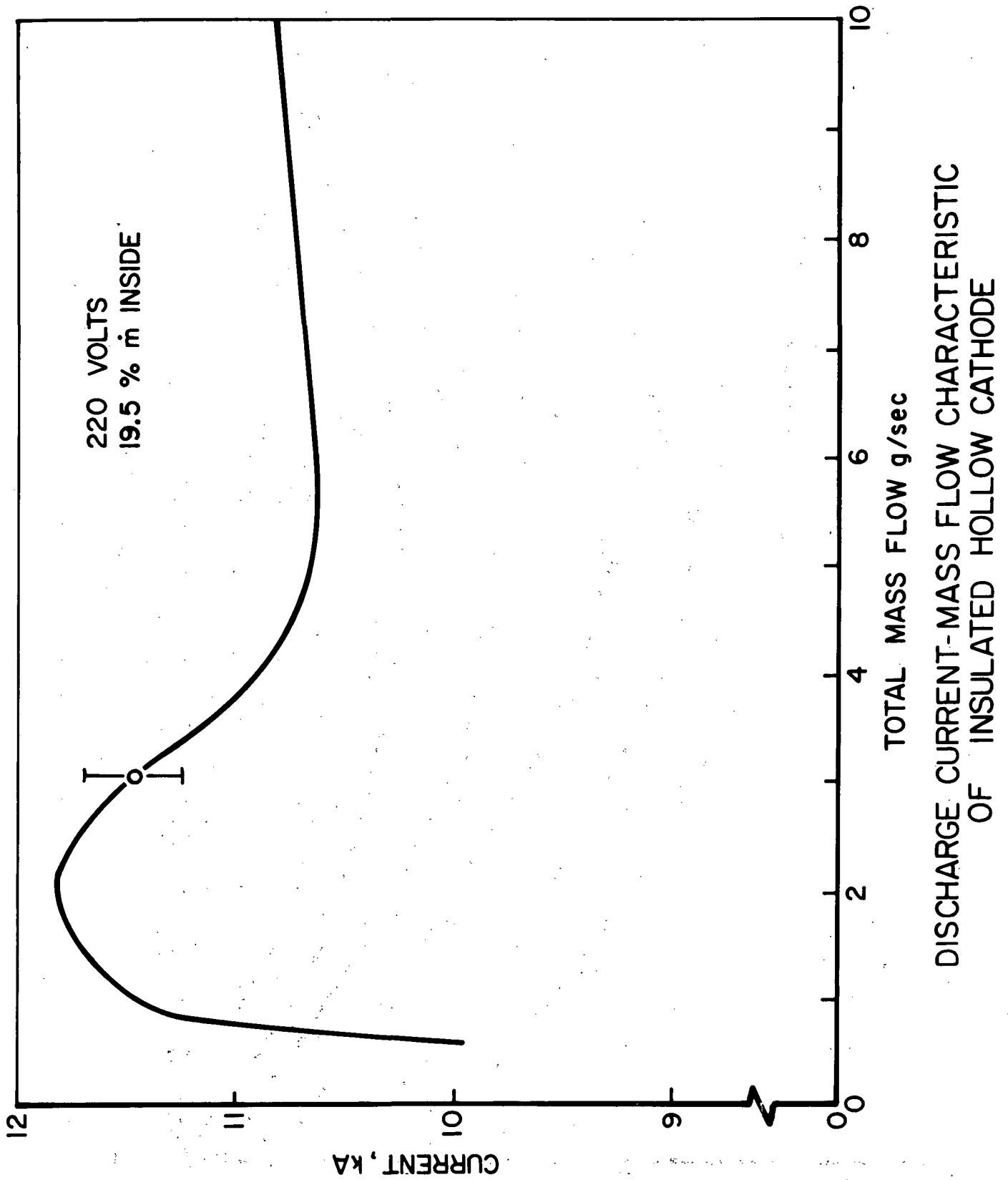
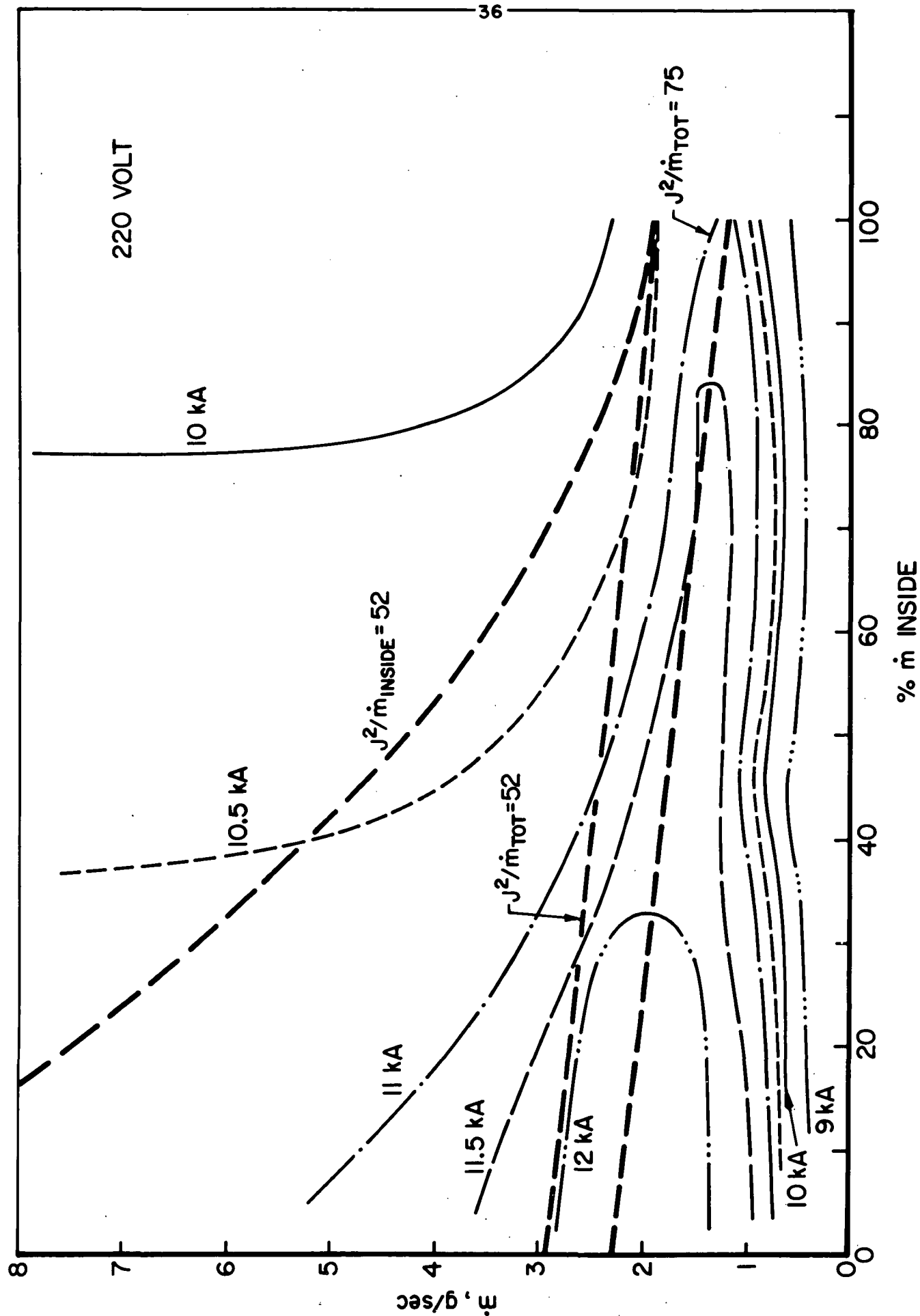


FIGURE 15
AP25-4725



DISCHARGE MASS FLOW CHARACTERISTICS
OF INSULATED HOLLOW CATHODE

a characteristic value. Above this characteristic value, the magnetoplasmadynamic operation becomes increasingly unstable and erratic, and the credibility of the corresponding MPD performance declines to the point of absurdity. This effect has been ascribed to the ingestion of spurious mass from either the electrodes, insulators, or previously exhausted propellant.

- The characteristic value of J^2/\dot{m} , where \dot{m} is the injected propellant only, is fairly well represented by

$$\left(\frac{J^2}{\dot{m}}\right)_{ch} = \left[(2 q N_o)^{1/2} / b \right] (\epsilon^i / M)^{1/2} \quad (\text{III-1})$$

where q = charge on an electron, C

N_o = Avogadro's number

ϵ^i = ionization energy

M = molecular weight

$$b = \frac{\mu_o}{4\pi} \left[\ln \left(\frac{r_+}{r_c} \right) + \text{constant} \right] \quad (\text{III-2})$$

$$\text{from} \quad F = b J^2 \quad (\text{III-3})$$

The parameter J^2/\dot{m} thus has a particular value for a given propellant and configuration. In our particular case, where argon is used as propellant, this formula can be written in a more practical form as follows:

$$\left(\frac{J^2}{\dot{m}}\right)_{ch} = 138 \left[\ln \left(\frac{r_+}{r_c} \right) + \frac{1}{2} \right]^{-1} \left(\frac{\epsilon^i}{M} \right)^{1/2} \quad (\text{III-4})$$

where J^2/\dot{m} is obtained in $\text{kA}^2\text{-sec-g}^{-1}$. These are the reasons that the lines of J^2/\dot{m} were also drawn on the graph. For comparison, a line of $J^2/\dot{m} = 52$ has also been drawn, which is the characteristic value calculated for this geometry from the simple argument based on an equipartition of energy between

kinetic and ionization modes (which is essentially the same as Malliaris). A similar line drawn for $J^2/\dot{m}_i = 52$ where \dot{m}_i is only that mass passing through the cathode, seems to bear little relation to any of the key features of the figure emphasizing that the total mass flow is a better scaling parameter for these terminal data.

A similar graph has been prepared for the tungsten hollow cathode and is shown in Fig. 17. A line of constant $J^2/\dot{m} = 56$, the calculated characteristic value for this configuration, coincides reasonably well with the locus of the optimum mass flows. For completeness, the results found for the conical hollow cathode are presented in Fig. 18. Here the calculated J^2/\dot{m} of 40 is compared to the locus of the optimum mass flows, which can be reasonably approximated by a line of $J^2/\dot{m} = 28$.

A first important observation from Fig. 16 is that this optimum mass flow decreases with higher flow fraction inside. The highest current of 12.5 kA was obtained for $\dot{m} = 2.1$ g/sec and 0% inside. However, for 100% inside the optimum occurs for a current of 11 kA, and only 1.2 g/sec. So for a reduction of current of about 15%, one has a reduction of mass flow of about 50%. Probably due to the earlier mentioned "anode effect" is the fact that the highest current point still occurs for 0% inside. J^2/\dot{m} for this point is 75, which doesn't quite correspond with the calculated characteristic value for argon of 52 for this configuration. This may be understood as if the discharge is not running on argon alone, but on a mixture of argon, carbon, hydrogen, and other ablated impurities. J^2/\dot{m}_a as a function of molecular weight is higher for the species with a lower atomic mass. Since carbon and hydrogen have a lower atomic mass, the higher value of $J^2/\dot{m} = 75$ could thus be explained. The hydrogen and carbon comes from ablation, especially from the nylon that was used as insulation of this particular cathode (HC-INS). The bell jar turned very black and also all the nylon insulation on the front of the cathode was ablated.

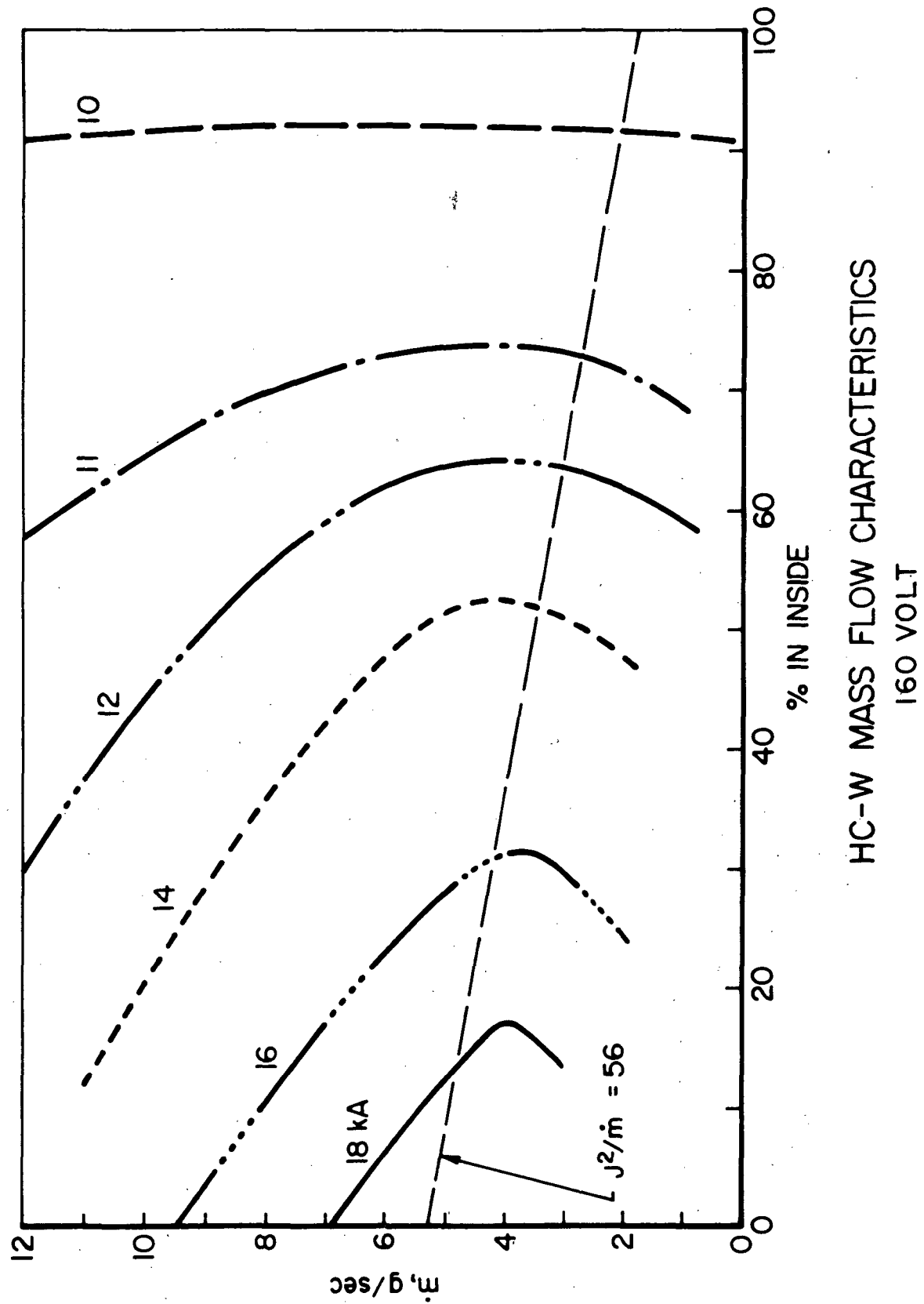
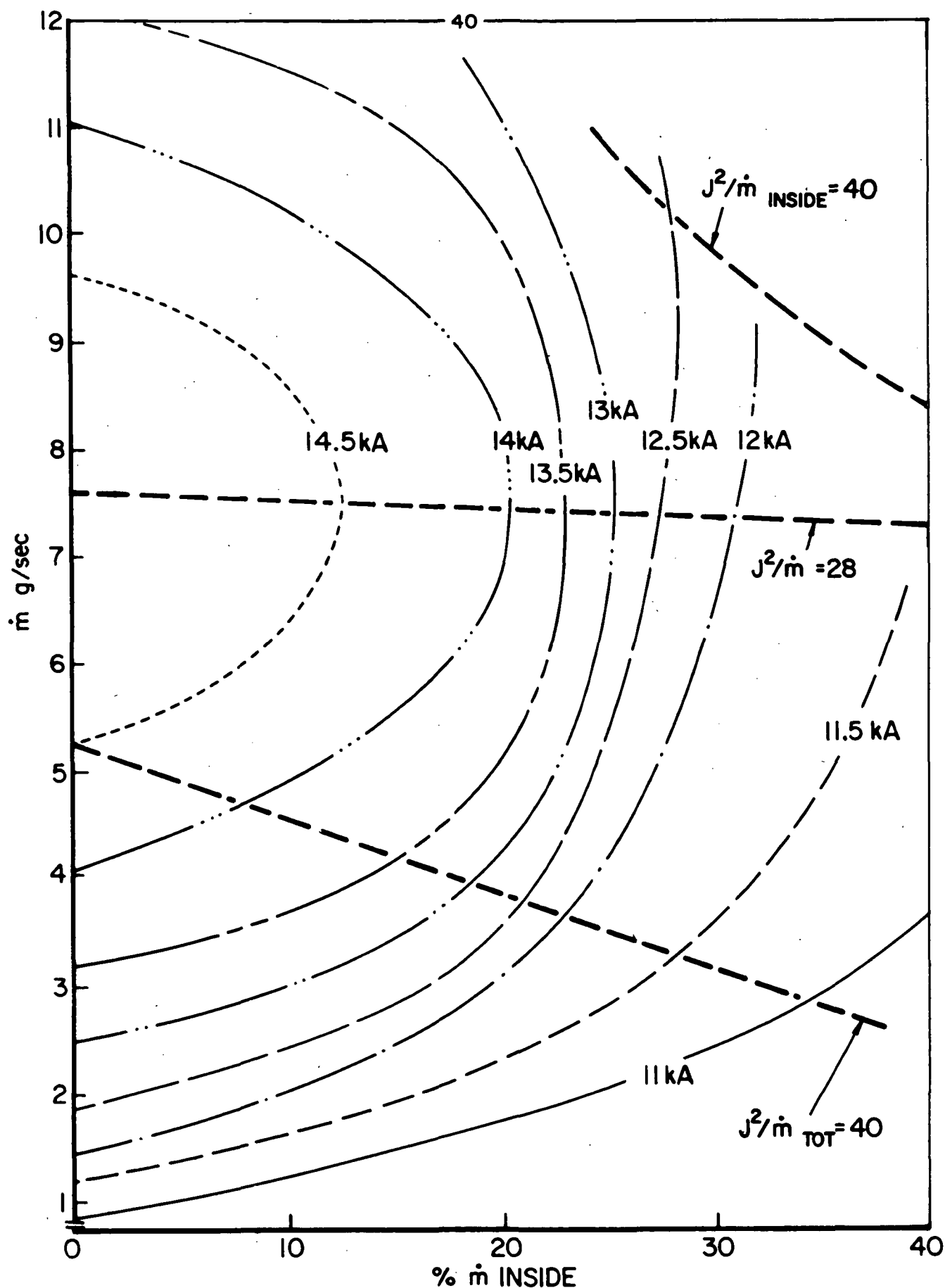


FIGURE 17
AP 25 4773 71



DISCHARGE CURRENT-MASS FLOW CHARACTERISTICS
OF THE CONICAL HOLLOW CATHODE

FIGURE 18

AP25 R 4722

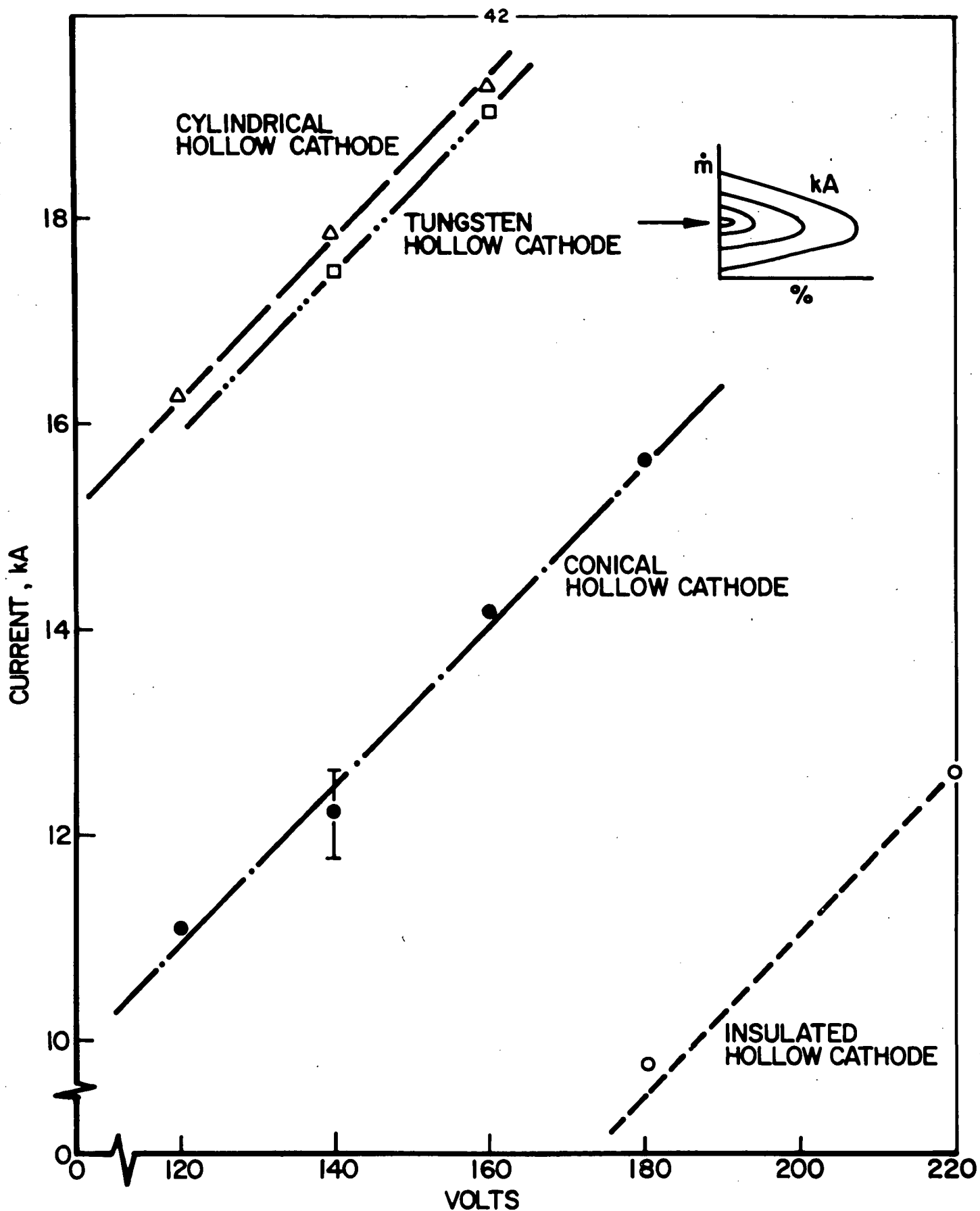
In Fig. 16, data points which lie above the $J^2/\dot{m} = 75$ line, i.e., mass flows greater than the optimum value, may indicate an overfed region, whereas those below the line may represent a region of starvation and subsequent mass ingestion. Thus the apparent insensitivity of the data to the initial flow distribution at low mass flows may be a manifestation of electrode or insulator erosion at these conditions.

It is of interest to know how this optimum (maximum current) that occurs for 0% inside varies as a function of voltage, since the previous graphs were made for a fixed voltage. Figure 19 exhibits this dependence as well as that for HC-SS, HC-CON, and HC-W. Noteworthy first is the rather large difference in current, of these optimum mass flows for the same voltage. Perhaps much more important is the fact that the slope for all of these cathodes is the same. This indicates that the discharge tends to run at a particular impedance, $\Delta V/\Delta J$, equal to 12.9 m Ω .

C. Dynamic Behavior of Discharge Voltage and Current

This is a study of the shape of the current and voltage traces as a function of time. It will be shown that certain features of these traces can be related to the parameter J^2/\dot{m} while others can be associated with hollow cathode operation.

For the electrolytic line, there is a distinct difference between the shape of the current traces for high current or low mass flow, i.e., high J^2/\dot{m} and those for low J^2/\dot{m} . Figures 20a, and 20b show that low J^2/\dot{m} tends to correspond to a current pulse shape resembling an exponential decay, while high J^2/\dot{m} agrees more with an initially flatter and rather smooth pulse shape. Even more important is the fact that there is little change in shape when the percent flow division is changed, as shown in Fig. 20c. This would imply that J^2/\dot{m}_{TOT} is a characteristic parameter for hollow cathode MPD discharges.



CHARACTERISTICS FOR OPTIMUM MASS FLOWS

1. The first part of the document discusses the importance of maintaining accurate records of all transactions and activities. It emphasizes the need for transparency and accountability in financial reporting.

2. The second part of the document outlines the various methods and techniques used to collect and analyze data. It includes a detailed description of the experimental procedures and the statistical analysis performed.

3. The third part of the document presents the results of the study. It includes a series of tables and graphs that illustrate the findings of the research. The data shows a clear trend in the relationship between the variables studied.

4. The fourth part of the document discusses the implications of the findings. It explores the potential applications of the research in various fields and the impact it may have on future studies.

5. The fifth part of the document provides a conclusion and summarizes the key points of the study. It reiterates the importance of the research and the need for further investigation in this area.

6. The sixth part of the document includes a list of references and a bibliography. It cites the works of other researchers in the field and provides a comprehensive overview of the literature related to the study.

7. The seventh part of the document contains a list of appendices and supplementary materials. These include additional data, figures, and tables that provide further detail and support for the findings of the study.

8. The eighth part of the document discusses the limitations of the study. It acknowledges the potential sources of error and the constraints of the experimental design.

9. The ninth part of the document provides a detailed description of the experimental setup and the equipment used. It includes a list of materials and a description of the procedures followed.

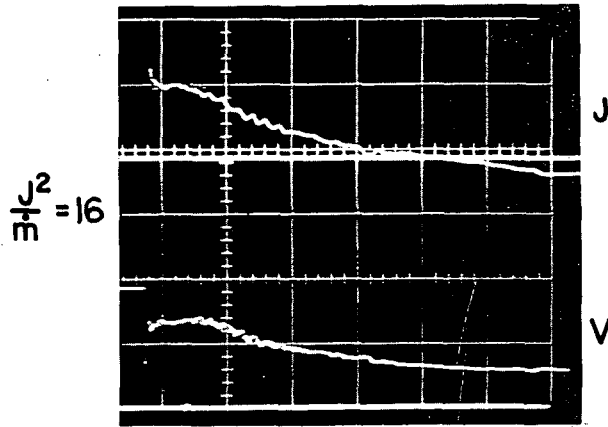
10. The tenth part of the document presents the results of the data analysis. It includes a series of tables and graphs that show the relationship between the variables studied.

11. The eleventh part of the document discusses the implications of the findings. It explores the potential applications of the research and the impact it may have on future studies.

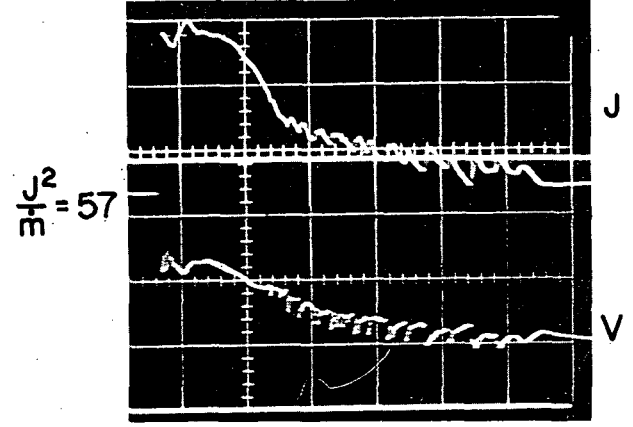
12. The twelfth part of the document provides a conclusion and summarizes the key points of the study. It reiterates the importance of the research and the need for further investigation in this area.

13. The thirteenth part of the document includes a list of references and a bibliography. It cites the works of other researchers in the field and provides a comprehensive overview of the literature related to the study.

14. The fourteenth part of the document contains a list of appendices and supplementary materials. These include additional data, figures, and tables that provide further detail and support for the findings of the study.

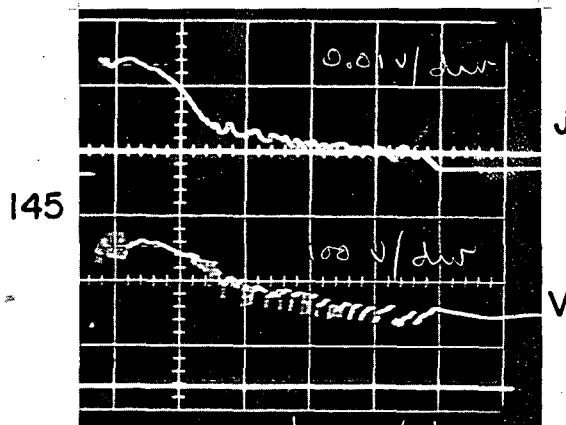


134 V, 5.8 kA

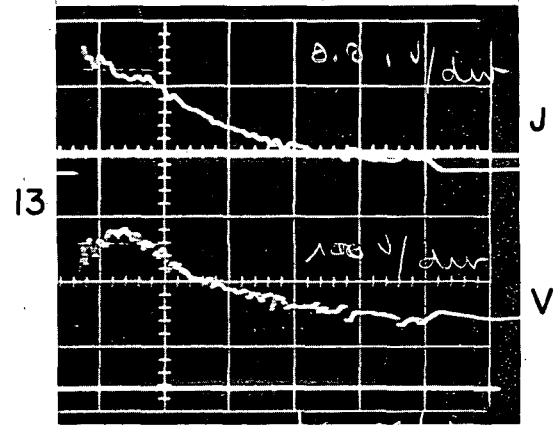


220 V, 10.9 kA

a) 2.1 g/sec, 45 % INSIDE

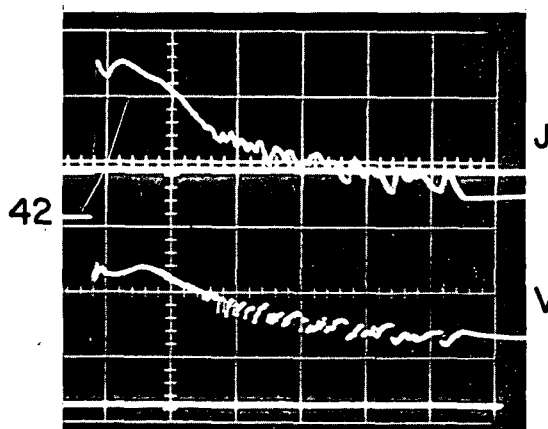


0.9 g/sec, 215 V, 11.5 kA

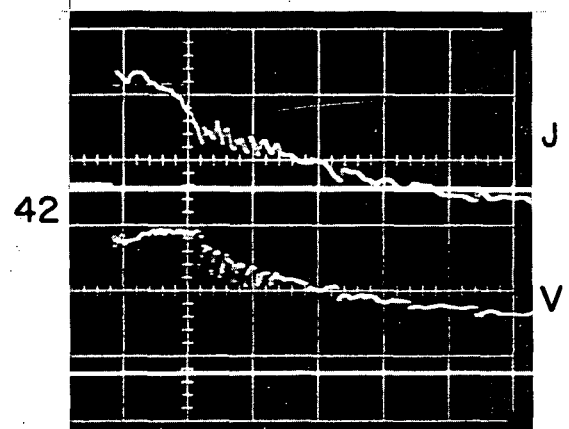


8.9 g/sec, 220 V, 10.9 kA

b) 69 % INSIDE



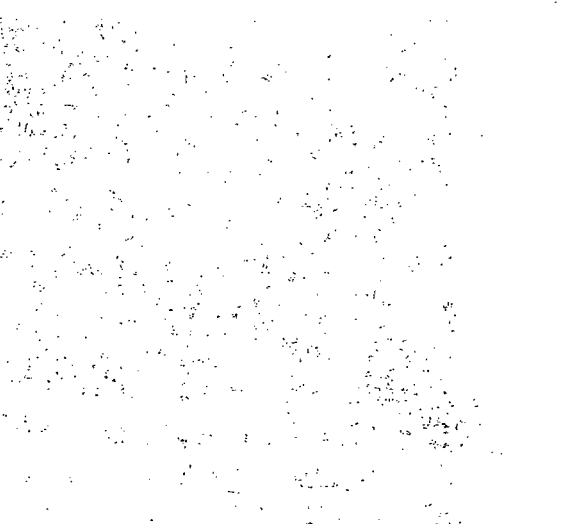
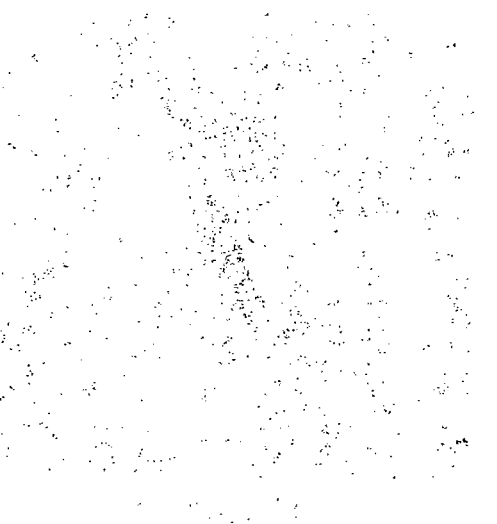
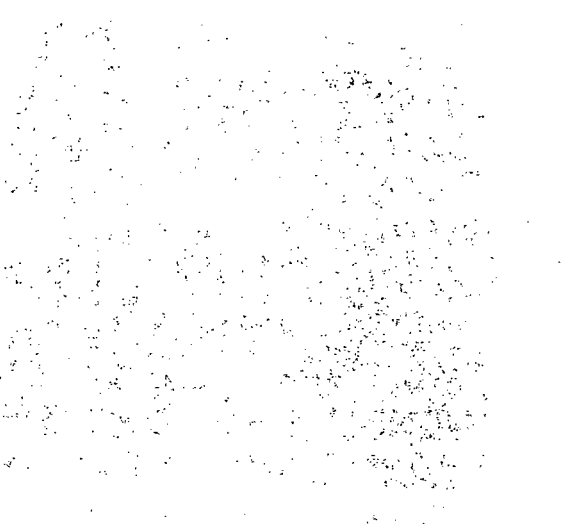
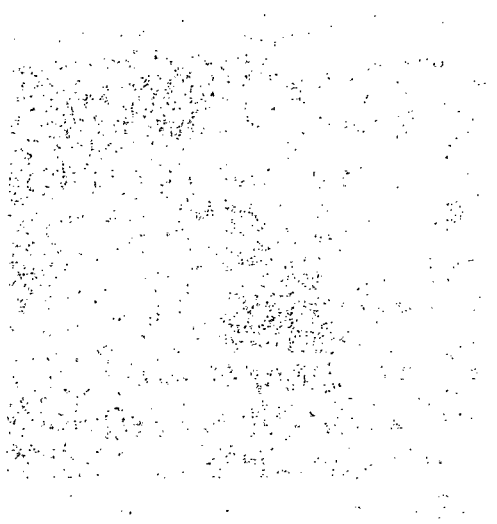
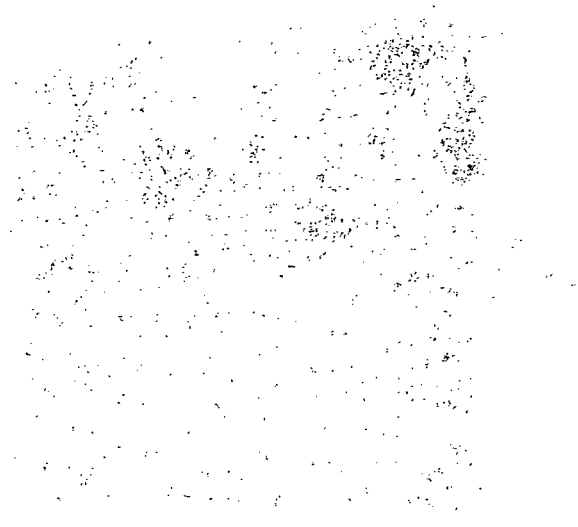
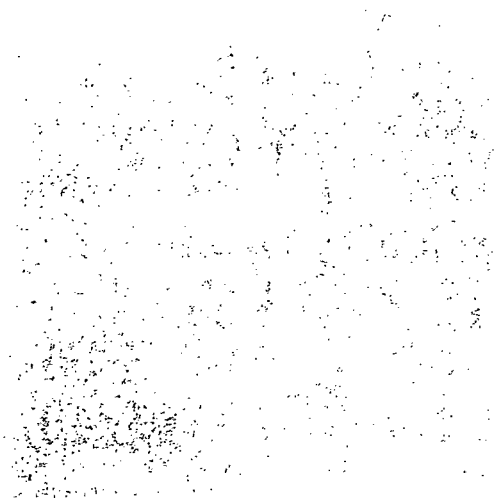
33%, 210 V, 9.6 kA



100%, 215 V, 9.3 kA

c) 2.1 g/sec

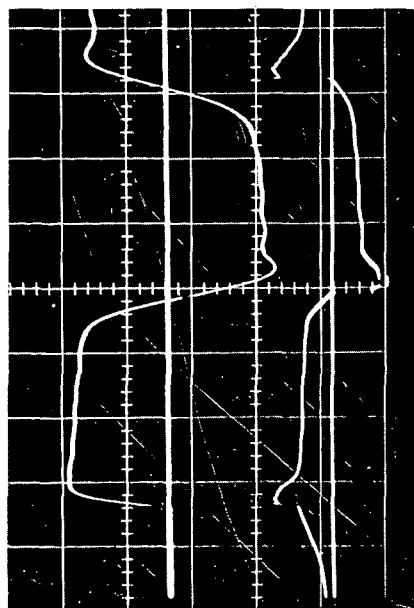
VOLTAGE AND CURRENT PROFILES
ELECTROLYTIC CAPACITOR BANK



That is, the total mass flow determines the characteristics of the discharge, rather than the mass flow outside or inside separately.

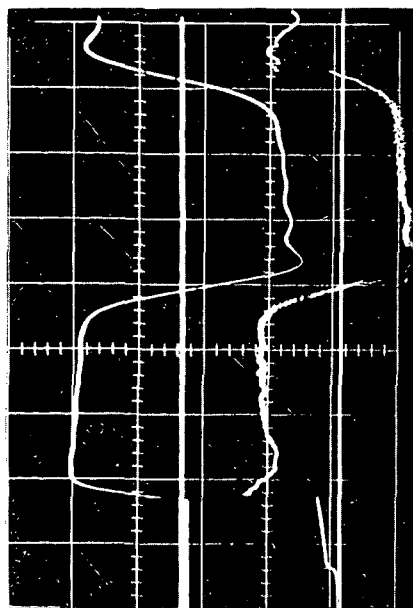
For the HC-SS, HC-CON and HC-INS, the electrolytic capacitor bank was used as the power supply. Then we switched to the high voltage capacitor line, where the current is fixed, to observe any change in the voltage shape when the HC-W was used. Figure 21 shows some typical data, on the left a total mass flow of 3.0 g/sec and 0% inside for a low current of 7.5 kA and high current 15.0 kA. To the right a total mass flow of 10.5 g/sec but 82% inside, again for a low 7.9 kA and high 15 kA current. For 0% inside we see that the discharge starts with a high voltage and drops to a lower, but steady voltage for both current levels. In the case of 82% inside, on the other hand, there is a drastic change. For the low current case, we have a voltage drop, during the start-up, whereas in the high current case, there is a rather sharp voltage rise. This change is not due to the current magnitude proved by the two pictures for a mass flow of 3.0 g/sec, neither to the mass flow outside, because otherwise Fig. 21c (3.0 g/sec) and Fig. 21d (10.5 g/sec total, 82% inside or 2.45 g/sec outside) would show the same trend, but mainly due to the mass flow inside the hollow cathode.

2 50 μ sec / DIV



a)

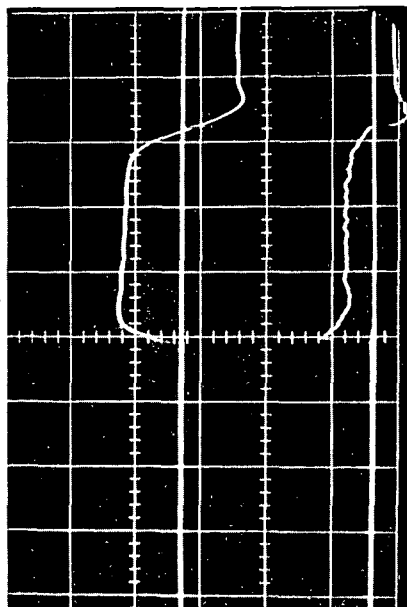
5



c)

$\dot{m} = 3.0$ g/sec
0% INSIDE

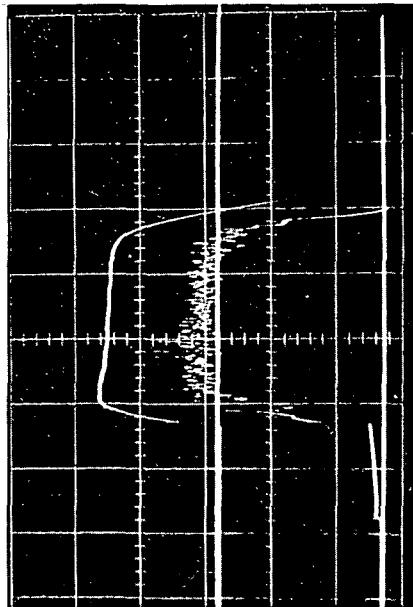
36



b)

J
4 kA / DIV
V
100 V / DIV

40



d)

$\dot{m} = 10.5$ g/sec
82% INSIDE

45

J
8 kA / DIV
V
100 V / DIV

FIGURE 21
AP25 P-414 71

HC-W CURRENT AND VOLTAGE PROFILES,
HIGH-VOLTAGE CAPACITOR BANK

CHAPTER IV

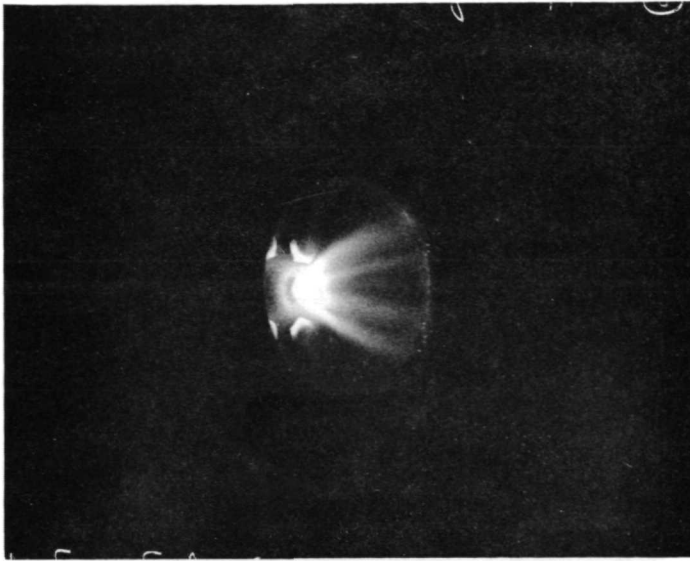
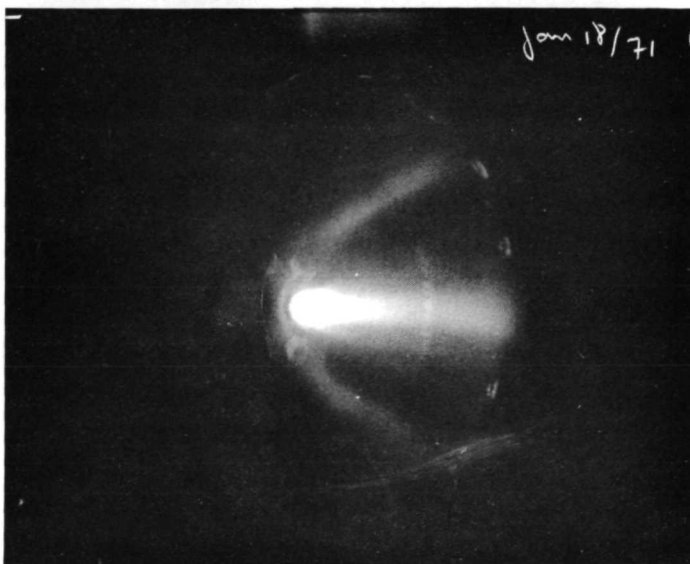
DISCUSSION

This chapter is concentrated on the physics of proper hollow cathode operation. Photographic observation showed that in some cases the most luminous part of the discharge was emerging from the cathode cavity, whereas for other conditions of current or mass flow the most luminous part was completely outside the orifice of the cathode. Two important parameters which influence the location of the discharge are the magnetic pressure and the gasdynamic pressure.

A. Magnetic Pressure

The significance of the magnetic pressure on the flow has been observed experimentally in the Kerr-cell photographs shown in Fig. 22. This illustration gives photographs of the quasi-steady discharge appearance with the HC-CON for three different currents, and a total mass flow of 6 g/sec of which 20% flows through the cathode. The HC-CON was selected, as mentioned before, for its large current densities and corresponding high magnetic pressures. As the current is increased from 9.2 kA in Fig. 22a to 13.2 kA in Fig. 22b, and to 14.1 kA in Fig. 22c, the originally expanding intensely radiating plasma flow in front of the cathode is seen to contract to a constricted cylindrical jet, under the influence of the higher magnetic pressure. This latter jet structure of the plasma is generally associated with proper hollow cathode operation.

For an evaluation of the magnetic pressure, attention is drawn to the approximate current distribution and consequent direction of the Lorentz force, as shown earlier in Fig. 5. On the outside of the hollow cathode, the body force, $\vec{f} = \vec{j} \times \vec{B}$, "blows" the fluid downstream and "pinches" the fluid radially inward. However, on the inside of the cavity, the

a) 90 V \times 9.2 kAb) 170 V \times 13.2 kAc) 190 V \times 14.1 kA

DISCHARGE WITH CONICAL HOLLOW CATHODE
(6 g/sec ARGON; 1.2 g/sec THROUGH CATHODE)

$\vec{j} \times \vec{B}$ force acts in the upstream direction.

On the inside, the effect of this body force and of the gasdynamical pressure is accounted for by the momentum equation which for the streaming direction, z , has the following form:

$$\rho u \frac{du}{dz} + \frac{dp}{dz} = -\frac{B}{\mu_0} \frac{dB}{dz} \quad (\text{IV-1})$$

where ρ = density
 u = velocity
 p = pressure

An immediate first integral of Eqn. (IV-1) is

$$(\rho u)u + p + \frac{B^2}{2\mu_0} = (\rho u)u_0 + p_0 + \frac{B_0^2}{2\mu_0} \quad (\text{IV-2})$$

where $B_0^2/2\mu_0$ is called the magnetic pressure. Thus, Eqn. (IV-2) expresses the conservation of the sum of total pressure plus momentum flux.

In order to make the problem one-dimensional, an average magnetic pressure over the area must be calculated. For a current density assumed uniform over the cross section of the cathode cavity, the magnetic field is axisymmetric and given by

$$B \, 2\pi r = \mu_0 j \pi r^2 \quad (\text{IV-3})$$

so that

$$B(r) = \frac{\mu_0 j r}{2} \quad (\text{IV-4})$$

With this expression, the average magnetic pressure over the cross section can be calculated from

$$\left(\frac{B^2}{2\mu_0} \right)_{av} = \frac{1}{\pi r_i^2} \int_0^{r_i} \frac{B(r)^2}{2\mu_0} 2\pi r dr \quad (\text{IV-5})$$

$$\left(\frac{B^2}{2\mu_0} \right)_{av} = \frac{\mu_0 j^2 r_i^2}{16} \quad (\text{IV-6})$$

where r_c is the radius of the hollow cathode cavity. This average magnetic pressure may now be compared to the gasdynamic pressure in the cavity as will be demonstrated in the next section.

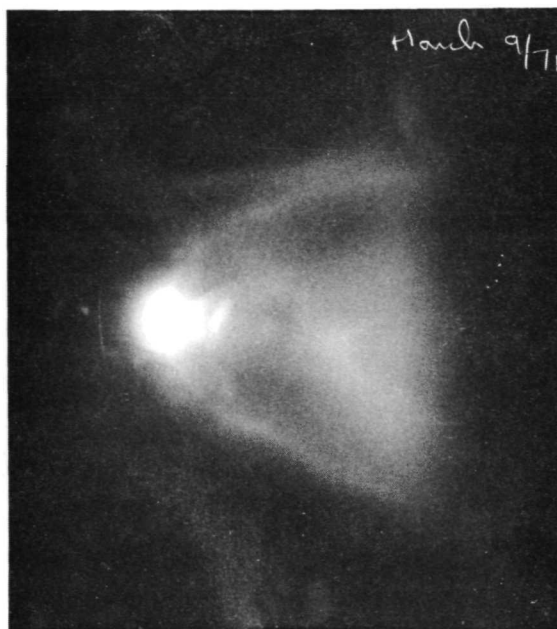
B. Gasdynamic Pressure

The gasdynamic pressure term in the momentum equation

$$\frac{B^2}{2\mu_0} + p + \rho u^2 = \text{constant} \quad (\text{IV-2})$$

is of equal importance for the plasma flow through the hollow cathode. Its influence is most evident in the case of the HC-INS, where the current is forced to attach on the inside. Figure 23 shows a series of 5 μ sec exposure Kerr-cell photographs taken during the quasi-steady operation of the discharge with the HC-INS. Since the current is nearly constant in these photographs, the variation of the $B^2/2\mu_0$ term will be small and thus the effect of the gasdynamic pressure can be observed. Observation of either pictures 23a and 23b, or pictures 23c and 23d, shows that for a fixed fraction of the flow inside, the exhaust pattern expands into a more "bell-shaped" radiant flow pattern as the mass flow is increased. In both cases the current and terminal voltages remain approximately the same.

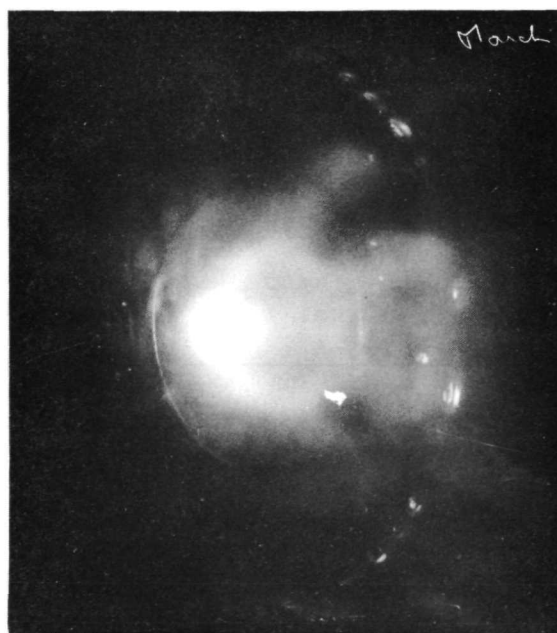
One possible explanation for these expanding flow patterns as the mass flow is increased or the fractional flow through the cathode is increased, is the ratio of the cavity pressure to the backpressure in the arc chamber. Since the reservoir pressure is of the order of atmospheres and the backpressure of the order of a few Torr for quasi-steady operation, it is obvious that the flow will choke at the minimum area through which the flow passes. For the present injection system, this minimum area occurs in the solenoid valve, of 0.4-cm-diameter. The flow will thus be supersonic through the 1.3-cm-diam cathode cavity, and the ratio of the cavity pressure to the reservoir pressure will be a constant determined by the ratio of the mentioned areas. When the reservoir pressure is increased



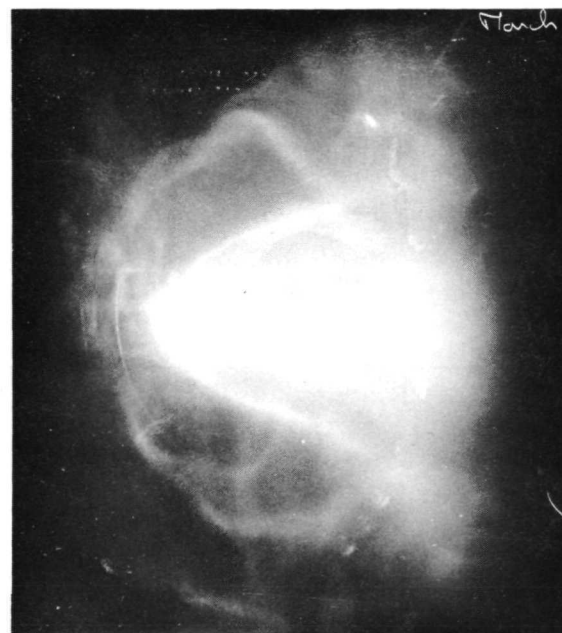
a) 220 V, 8.8 kA, 2.9 g/sec, 100% INSIDE



b) 215 V, 10 kA, 9.1 g/sec, 100% INSIDE



c) 220 V, 11.3 kA, 0.9 g/sec, 19.6 % INSIDE



d) 220 V, 10.8 kA, 8.9 g/sec, 19.6% INSIDE

KERR CELL PHOTOGRAPHS OF
HC-INS DISCHARGE

FIGURE 23
AP25 P-393 71

to augment the mass flow, the cavity pressure linearly follows this rise. Since it has been shown that the arc chamber pressure is only very weakly dependent on the total mass flow for this operating regime, the ratio of cathode cavity pressure to chamber backpressure also rises supporting the observed flow expansion at higher mass flows.

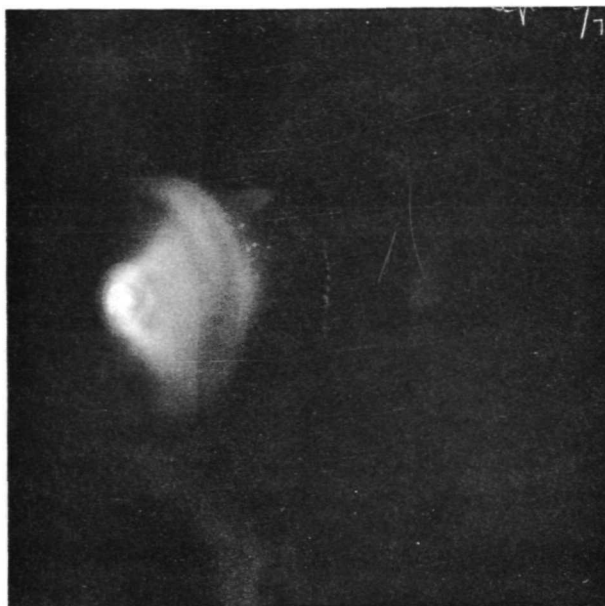
The greater expansion observed for the same current and total mass flow, but with all the flow passing through the cathode cavity in Fig. 23b as compared to Fig. 23d with only 20% of the flow through the cavity, may be explained again by an increased cavity pressure. In this case, however, the pressure increase is due to the smaller effective expansion area ratio to permit the increased flow through the cavity.

The ohmic energy deposition within the cavity deserves consideration because it also will increase the pressure. Ohmic power input will depend strongly on the details of the cathode emission mechanisms since these mechanisms dictate the potential profiles and current distribution within the cavity. Only when the potential and current distributions are determined experimentally over the entire cathode surface will the magnitude of the power deposition be realized, and thus the latter's contribution to the photographs in Fig. 23 is presently unknown.

Gasdynamic pressure has another important role in the behavior of a hollow cathode. We have discussed the magnetic force acting in the upstream direction, inside the hollow cathode. If gasdynamic pressure is higher than the magnetic pressure, it is possible that the unbalanced forces will drive the current attachment downstream and eventually outside of the hollow cathode. Thus, to first order, to keep the discharge inside the hollow cathode, the magnetic pressure averaged over the front surface has to be equal to the gasdynamic pressure, taking into account also the pressure increase due to ohmic energy deposition.

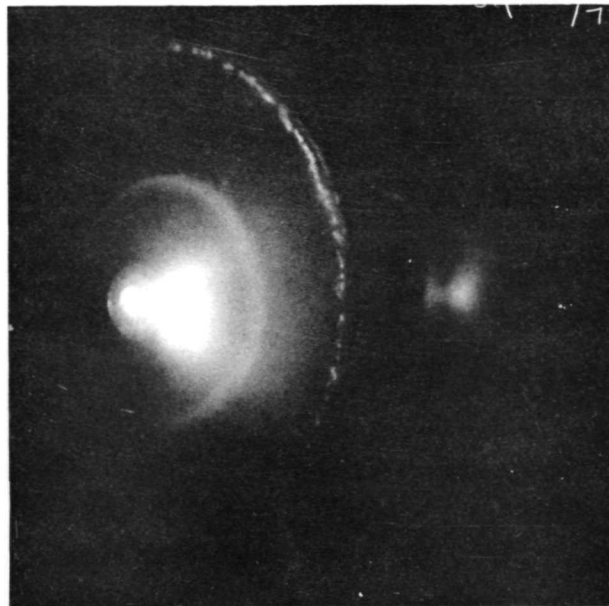
This is verified in a series of 5 μ sec Kerr-cell photographs taken at different times during the initiation of the pulse. Figure 24 shows a sequence of typical pictures of the start of the discharge with the tungsten hollow cathode for

1



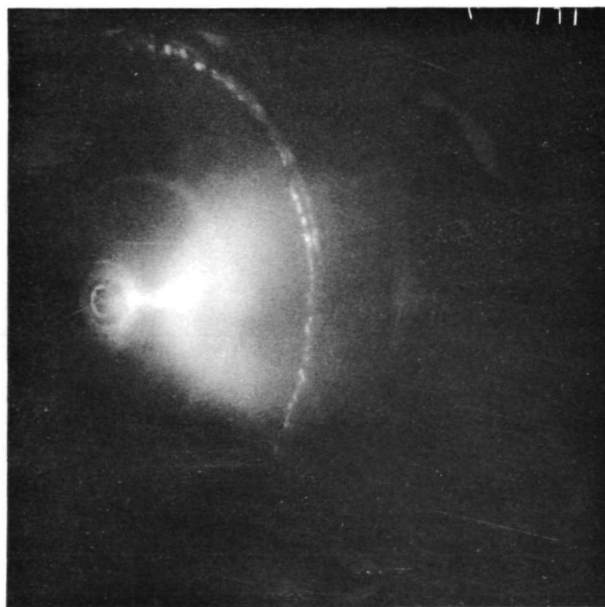
a) 1.8 kA , 143 V
1.5 μ sec

5



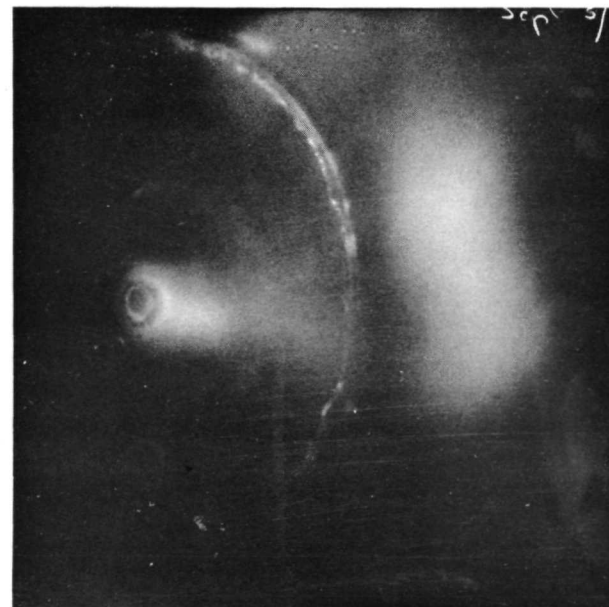
b) 11 kA , 195 V
8.7 μ sec

8



c) 14.7 kA , 240 V
16.5 μ sec

9



d) 15 kA , 290 V
30 μ sec

STARTING SEQUENCE WITH TUNGSTEN HOLLOW CATHODE
 $\dot{m} = 7.9$ g/sec , 82 % INSIDE

FIGURE 24
AP25-P 412

a total mass flow of 7.9 g/sec of which 82% is inside. The discharge starts on the inside, where a luminous plasma is observed in Fig. 24a. It is important to mention that this observation is not a special case, but is recorded for a large range of current levels and mass flow rates. This initiation of the discharge may be related to a higher neutral density inside the cavity providing the required product of pressure and gap spacing for breakdown. After several microseconds, a luminous plasma is seen to be expelled from the hollow cathode, Fig. 24b and 24c. This may be because the gasdynamic pressure is increased inside the hollow cathode by the heating, and so overwhelms the rather small magnetic pressure. Afterwards this plasma expands and is accelerated downstream. At later times, Fig. 24d, it is observed that the current attachment moves from the inside to the front surface, where it stays during the quasi-steady part of the discharge.

CHAPTER V

SUMMARY

In this study four different types of hollow cathode have been tested. The terminal voltage and total current were monitored with regard to their behavior as a function of other arc parameters, such as total mass flow and fraction of the mass flow through the cathode. For a fixed voltage and fixed fraction of the mass flow inside, the current increases with total mass flow rate up to a certain point, and then drops. For higher mass flows the current seems independent of mass flow. This optimum may distinguish "overfed" and "underfed" MPD operating conditions. The discharge characteristics also provide evidence that both inside and outside gas flows contribute to the discharge phenomena. In comparison to the conventional conical cathode where the terminal voltage decreases with increasing mass flow rate for a fixed current, the hollow cathode voltage increases with mass flow rate. Two controlling parameters of a hollow cathode are the magnetic pressure and gas-dynamic pressure inside the cavity. It is asserted that in order to keep the discharge inside the hollow cathode these two have to balance. This was also shown by interpretation of photographs of the discharge taken during the starting transient and steady regions. Finally, it was verified that the parameter J^2/\dot{m} is significant for scaling arc operation, but may not be the only parameter of significance for the hollow cathode discharge.

APPENDIX

CALCULATION OF THE MEAN FREE-PATH

For calculating the parameters K_1 and K_2 , which are the ratios of the mean-free-path for ionization of incoming propellant atoms by electrons to the length and diameter of the cathode cavity respectively, the mean-free-path is calculated from

$$\lambda_i = \frac{v_a}{v_{ae}^i} = \frac{\text{atom velocity}}{\text{collision frequency for ionization by an electron}} \quad (\text{II-4})$$

in which the collision frequency v_{ae}^i is expressed as the following:^{A-2}

$$v_{ae}^i = \propto n_{eo} \left(\frac{2}{\pi}\right)^{1/2} \left(\frac{m_e}{kT_e}\right)^{3/2} e^{-\frac{m_e v_t^2}{2kT_e}} \times \quad (\text{II-6})$$

$$\left[\left(\frac{2kT_e}{m_e}\right)^3 + \frac{3}{2} v_t^2 \left(\frac{2kT_e}{m_e}\right)^2 + v_t^4 \left(\frac{2kT_e}{m_e}\right) \right]$$

The number density of argon is estimated by considering an efflux of neutral gas from a cylindrical orifice. Also the external pressure in the vacuum-vessel (about 10^{-6} torr) is considered negligible, with respect to the pressure at the tip of the cavity. Therefore a strong pressure gradient exists in front of the orifice. The arrival rate of atoms \dot{N}_a is

$$\dot{N}_a = \frac{1}{4} n_a \bar{v}_a A_c \quad (\text{A-1})$$

$$\dot{N}_a = \frac{1}{4} n_a \left(\frac{8kT}{\pi m_a} \right)^{1/2} A_c \quad (\text{A-2})$$

in which T is the absolute temperature ($^{\circ}\text{K}$) and \bar{v}_a is the average thermal velocity.

For the case of argon with the assumption of a temperature of approximately 10 eV, the average thermal velocity \bar{v}_A becomes

$$\bar{v}_A = \left(\frac{8kT}{\pi m_A} \right)^{1/2} = 7.76 \times 10^4 \text{ cm/sec} \quad (\text{A-3})$$

The number density n_A is

$$n_A = \frac{4 \dot{m}_A}{\bar{v}_A A_c m_A} \quad (\text{A-4})$$

This number density will vary over a wide range due to variation in \dot{m} and A . Consider an orifice of 0.64-cm-diam which gives us an area of $A_c = 0.316 \text{ cm}^2$. Assuming that the mass flow through the hollow cathode corresponds to an equivalent current of 20% of the total current, then for a total current $J = 10,000 \text{ A}$, the equivalent current is 2000 A. The mass flow \dot{m} is then

$$\dot{m}_A = (0.2) \frac{J m_A}{q} \quad (\text{A-5})$$

where q is the electron charge. This gives us:

$$\dot{m}_A = 0.82 \text{ g/sec} \quad (\text{A-6})$$

and so the number density is

$$n_A = 1.72 \times 10^{22} \text{ particles/m}^3$$

For Argon

$$\varepsilon_t = 15.7 \text{ eV}$$

$$\varepsilon_{\max} = 50 \text{ eV}$$

$$Q_{\max} = 3.21 \times 10^{-20} \text{ m}^2$$

$$\alpha = 0.266 \times 10^{-32} \text{ sec}^2$$

v_t was the velocity where electrons energy (as kinetic energy) is at threshold for ionization of argon.

$$\frac{m_e v_t^2}{2} = 15.7 \text{ eV} = \varepsilon_t$$

$$m_e = 9.11 \times 10^{-31} \text{ kg}$$

and $v_t = 2.3 \times 10^6 \text{ m/sec}$

With these numbers substituted in the formula for the collision frequency ν_{Ae}^i :

$$\nu_{Ae}^i = 6.4 \times 10^7 \text{ sec}^{-1}$$

The mean-free-path for ionization

$$\lambda^i = \bar{v}_A / \nu_{Ae}^i$$

$$\bar{v}_A = 7.76 \times 10^4 \text{ cm/sec}$$

$$\nu_{Ae}^i = 6.4 \times 10^7 \text{ sec}^{-1}$$

$$\lambda^i = 1.22 \times 10^{-3} \text{ cm}$$

is indeed seen to be small with respect to the cathode dimensions.

HOLLOW CATHODE REFERENCES
(Chronological Listing)

1. Weinstein, R. H., and Hess, R. V., "New Experiments with Hollow Cathode Discharges," Proceedings of the Third Symposium on Engineering Aspects of Magnetohydrodynamics, March 1962.
2. Lidsky, L. M., Rothleder, S. D., Rose, D. J., and Yoshikawa, S., "Highly Ionized Hollow Cathode Discharge," Journal of Applied Physics, Vol. 33, No. 8, August 1962, pp. 2490-2497.
3. Morley, J. R., "The Hollow Cathode Discharge," Proceedings of the Fifth Annual Meeting of the Electric Beam Symposium, March 1963.
4. Bade, W. L. and Yos, J. M., "Theoretical and Experimental Investigation of Arc-Plasma Generation Technology, Part II, Vol. 1, A Theoretical and Experimental Study of Thermionic Arc Cathodes," ASD-TDR-62-729, September 1963, Aeronautical Systems Division, Wright-Patterson, Ohio.
5. Klementev, V. M., "Large Radius Hollow Cathode with Uniform Discharge Over the Cross Section," UDC 537-525, March-April 1965, Academy of Sciences, USSR.
6. Roberts, Jr., A. S., and Bennett, W. H., "Plasma Temperature Measurements for the Hollow Cathode Discharge," Journal of Applied Physics, Vol. 35, No. 12, December 1964, pp. 3434-3436.
7. Morse, D. L., "Plasma Rotation in a Hollow Cathode Discharge," The Physics of Fluids, Vol. 8, No. 3, March 1965, pp. 516-521.
8. Lidsky, L. M., "Plasma Generation in the Hollow Cathode Discharge," Nuclear Engineering Department and Research Laboratory of Electronics, Massachusetts Institute of Technology, Cambridge, Mass., 1965.
9. Weinstein, R. H. and Hoell, James M., "Experiments in a Hollow Cathode Hall Current Accelerator," AIAA Paper 65-299, San Francisco, Calif., 1965.
10. Znamenskii, V. B., Buinov, G. N. and Bursakov, E. S., "Investigation of the Dependence of the Discharge Parameters and Generating Power of the He-Ne Laser on the Hollow Cathode Diameter," UDC 621-375-9:535, pp. 292-293.

HOLLOW CATHODE REFERENCES

11. Moskalev, B. I., "Striations in a Hollow Cathode Plasma," Soviet Physics - Technical Physics, Vol. 10, No. 8, February 1966.
12. Popovici, C., and Somesan, M., "On the Emission Spectrum of the Negative Glow Plasma of a Hollow Cathode Discharge in a Magnetic Field," Applied Physics Letters, Vol. 8, No. 5, March 1966, pp. 103-105.
13. Borodin, V. S. and Kagan, Y. M., "Investigation of Hollow Cathode Discharge. I. Comparison of the Electric Characteristics of a Hollow Cathode and a Positive Column," Soviet Physics - Technical Physics, Vol. 11, No. 1, July 1966, pp. 131-134.
14. Borodin, V. S., Kagan, Y. M. and Lyagushchenko, R. I., "Investigation of a Hollow Cathode Discharge. II." Soviet Physics - Technical Physics, Vol. 11, No. 7, January 1967, pp. 887-889.
15. Hoell, J. M. and Brooks, D. R., "Effect of Propellant Injection through Electrodes on Potential Distribution in an MPD arc," AIAA Paper 67-49, New York, 1967.
16. Brooks, D. R., Hoell, J. M., Jr., Hess, R. V. and Brockman, P., "Diagnostics and Interpretation of Acceleration Mechanisms in an MPD Arc," AIAA Paper 67-676, Colorado Springs, Colorado, 1967.
17. Ward, J. W. and King, H. J., "Mercury Hollow Cathode Plasma Bridge Neutralizers," Journal of Spacecraft and Rockets, Vol. 5, No. 10, October 1968, pp. 1161-1164.
18. Rawlin, V. K. and Pawlik, E. V., "A Mercury Plasma-Bridge Neutralizer," Journal of Spacecraft and Rockets, Vol. 5, No. 7, July 1968, pp. 814-820.
19. Bechtel, R. T., Csiky, G. A., and Byers, D. C., "Performance of a 15-cm Diameter, Hollow Cathode Kaufman Thruster," AIAA Paper 68-88, New York, 1968.
20. Philip, C. M., "A Study of Hollow Cathode Discharge Characteristics," Space Department, Royal Aircraft Establishment, Hampshire, England, 1969.

HOLLOW CATHODE REFERENCES

21. Borodin, V. S., Gofmeyster, V. and Kagan, Y. M., "Investigation of a Discharge in a Hollow Cathode," FTD-MT-24-264-69, 1969, Foreign Technology Division, Air Force.
22. Fradkin, D. B., Blackstock, A. W., Roehling, D. J., Stratton, T. F. and Williams, M., "Experiments Using a 25 kW Hollow Cathode Lithium Vapor MPD Arc Jet," AIAA Paper 69-241, Williamsburg, Va., 1969.
23. Csiky, G. A., "Investigation of a Hollow Cathode Plasma," AIAA Paper 69-258, Williamsburg, Va., 1969.
24. Csiky, G. A., "Measurements of Some Properties of a Discharge from a Hollow Cathode," TN D-4966, February 1969, NASA.
25. Esker, D. W., Kroutil, J. C. and Checkley, R. J., "Radiation Cooled MPD Arc Thruster," CR 72557, July 1969, NASA.
26. Byers, D. C., "Effect of Power Supply Impedance on the SERT II Neutralizer," TMX-52543, 1969, NASA.
27. Rawlin, V. K. and Kerslake, W. R., "Durability of the SERT II Hollow Cathode and Future Applications of Hollow Cathodes," AIAA Paper 69-304, Williamsburg, Va., 1969.
28. Bechtel, R. T., "Performance and Control of a 30-cm Diameter Low Impulse Kaufman Thruster," AIAA Paper 69-238, Williamsburg, Va., 1969.
29. Holt, J. F. and Boyes, E. L., "Experimental Study of a Hollow Cathode Argon Arc Plasma," AFAPL-TR-69-76, September 1969, Air Force Aero Propulsion Laboratory, Ohio.
30. Westinghouse, "Hollow Cathode Discharge Devices," Supersedes TD 86-375, ET-1532, ET-1553, ETD-6503, April 1970.
31. Bechtel, R. T., "Component Testing of a 30-cm Diameter Electron Bombardment Thruster," AIAA Paper 70-1100, Stanford, Calif., 1970.
32. Kretschmen, C. B., "Analytical and Diagnostic Research in High Temperature Plasma Transverse Ion Energies in Gas Fed Hollow Cathode Arcs," ARL 70-0243, October 1970, Aerospace Research Laboratories.

HOLLOW CATHODE REFERENCES

33. Byers, D. C. and Snyder, A., "Parametric Study of Mercury Hollow Cathode Neutralizers," AIAA Paper 70-1090, Stanford, Calif., 1970.
34. Reader, P. D., Nakanishi, S., Lathem, W. C. and Banks, B. A., "A Sub-millipound Mercury Electron Bombardment Thruster," AIAA Paper 70-616, San Diego, Calif., 1970.
35. Byers, D. C. and Snyder, A., "Parametric Investigation of a Mercury Hollow Cathode Neutralizer," TM X-52835, 1970, NASA.
36. Bechtel, R. T., "Component Testing of a 30-cm Diameter Electron Bombardment Thruster," AIAA Paper 70-1100, Stanford, Calif., 1970.
37. Jahn, R. G., von Jaskowsky, W. F. and Clark, K. E., "Pulsed Electromagnetic Gas Acceleration," semi-annual report for period 1 July 1970 to 31 December 1970, Aerospace and Mechanical Sciences Rept. No. 634p, January 1971, Princeton University, Princeton, N. J.
38. Kroutil, J. C., Esker, D. W., Sedrick, A. V., "Cathode Studies of a Radiation Cooled MPD Arc Thruster," CR 72891, May 1971, NASA.
39. Burkhart, J. A., "Exploratory Tests on a Downstream Cathode MPD Thruster," Journal of Spacecraft and Rockets, Vol. 8, No. 3, March 1971, pp. 240-244.
40. Bessling, H., "Hohlkathodenuntersuchungen," Vortrag Nr. 71-045, DGLR Symposium Elektrische Antriebsysteme, Braunschweig, June 1971.
41. NASA Literature Search, "Hollow Cathode Gas Discharges," National Aeronautics and Space Administration, Literature Search Number 15888, July 1971, NASA.
42. Goldstein, R., Pawlik, E. V., and Chi Wen, L., "Preliminary Investigation of Ion Thruster Cathodes," Tech. Rept. 32-1536, August 1971, Jet Propulsion Laboratory, California Institute of Technology, Pasadena, Calif.
43. Kerslake, W. R., Goldman, R. G., and Nieberding, W. C., "SERT II, Mission, Thruster Performance, and In-Flight Thrust Measurements," Journal of Spacecraft and Rockets, Vol. 8, No. 3, March 1971, pp. 213-234.

HOLLOW CATHODE REFERENCES

44. Reader, P. D. and Kerslake, W. R., "Bombardment Thruster Investigation at the Lewis Research Center - 1971," TMX 67836, May 1971, NASA.
45. Csiky, G. A., "Langmuir Probe Measurements in a SERT II Thruster Discharge Chamber," TMX 2088, January 1971, NASA.
46. Byers, D. C., Reader, P. D., "Electron Bombardment Ion Source Operation Using Various Gases," TMX-67831, May 1971, NASA.
47. Nakanishi, S., Lathem, W. C., Banks, B. A. and Weigand, A. J., "Performance of a Submillipound Mercury Electron Bombardment Thruster Subsystem," AIAA Paper 71-690, Salt Lake City, Utah, June 1971.
48. Jahn, R. G., von Jaskowsky, W. F. and Clark, K. E., "Pulsed Electromagnetic Gas Acceleration," semi-annual report for period 1 January 1971 to 30 June 1971, Aerospace and Mechanical Sciences Rept. No. 634q, July 1971, Princeton University, Princeton, N. J.

GENERAL REFERENCES

- A-1 Jahn, R. G., Physics of Electric Propulsion, McGraw Hill Book Company, New York, 1968.
- A-2 Turchi, P. J. and Jahn, R. G., "The Cathode Region of a Quasi-steady Magnetoplasmdynamic Arcjet," Aerospace and Mechanical Sciences Rept. No. 940, October 1970, Princeton Univ., Princeton, N. J.
- A-3 Oberth, R. C. and Jahn, R. G., "Anode Phenomena in High-Current Discharges," Aerospace and Mechanical Sciences Rept. No. 961, December 1970, Princeton Univ., Princeton, N. J.
- A-4 Jahn, R. G., von Jaskowsky, W. F. and Clark, K. E., "Pulsed Electromagnetic Gas Acceleration," semi-annual report for period 1 January 1971 to 30 June 1971, Aerospace and Mechanical Sciences Rept. 634q, July 1971, Princeton Univ., Princeton, N. J.
- A-5 Malliaris, A. C., John, R. R., Garrison, R. L. and Libby, D. R., "Quasi-steady MPD Propulsion at High Power," CR-111872, February 1971, NASA.